ADAPTIVE DYNAMICS OF SCATTERERS IN MULTI-FREQUENCY LIGHT FIELDS IN OPTICAL RESONATORS

Masterarbeit

zur Erlangung des akademischen Grades
Master of Science (MSc)

an der
Fakultät für Mathematik, Informatik und Physik
der
Leopold-Franzens-Universität Innsbruck

vorgelegt von

Valentin Torggler

Betreuer:
Univ.-Prof. Dr. Helmut Ritsch

Innsbruck, im November 2014

Danksagung

Zuerst möchte ich mich bei Helmut Ritsch für die Betreuung dieser Arbeit bedanken. Mit physikalischer Intuition, Wissen und Erfahrung motivierte und leitete er mich zur Bewältigung dieser Aufgabe. Dabei wurde es mir ermöglicht an Konferenzen teilzunehmen und ein Paper zu veröffentlichen. Auch hervorzuheben ist die positive und kollegiale Atmosphäre in seiner Forschungsgruppe.

Außerdem danke ich Wolfgang Niedenzu, Sebastian Krämer, Stefan Ostermann und Michael Schuler für fachliche Diskussionen, praktische Tipps und Hilfe bei Computerproblemen, Raimar Sandner, der es mir ermöglicht hat am Young European Scientists Meeting am Venet bei Landeck teilzunehmen und meinen Bürokollegen Daniela Holzmann und Dominik Winterauer für die unterhaltsame Koexistenz.

Zu guter Letzt möchte ich meiner Familie und meinen Freunden danken, speziell jedoch meinen Eltern, die mich immer moralisch und finanziell unterstützt und mir damit das Studium ermöglicht haben.

Zusammenfassung

Photonen besitzen nicht nur Energie sondern auch Impuls und üben daher Kräfte auf materielle Teilchen aus. Füllt man einen optischen Fabry-Pérot-Resonator mit polarisierbaren Teilchen (Atome, Moleküle oder Nano-Teilchen) und bestrahlt diese transversal mit Laserlicht verursachen diese Kräfte eine komplexe Dynamik. Die Teilchen streuen das Licht in den Resonator und erzeugen damit gleichzeitig ihre eigene optische Falle. Um ihre Energie zu minimieren, gehen sie von einer homogenen in eine regelmäßige, kristalline Anordnung über, wodurch die Streuung maximiert und ein tiefes optisches Potential erzeugt wird. Über Verluste durch die Spiegel können die Teilchen kinetische Energie abgeben („cavity cooling“) und der geordnete Zustand wird stabil. Diese Selbstorganisation von polarisierbaren Teilchen in Resonatoren ist im Fall von nur einem monochromatischen Laser-Pumpstrahl bereits bekannt und experimentell nachgewiesen.

In dieser Arbeit simulieren wir die dynamische Entwicklung der Teilchen unter gleichzeitiger Beleuchtung mit mehreren Frequenzen die in verschiedenste Lichtmoden unterschiedlicher Frequenz gestreut werden. Die Lichtfelder dieser Moden konkurrieren nun darum, die Teilchen in die jeweils für sie günstigste Anordnung zu drängen. Diese Dynamik endet in einem stabilen Gleichgewicht, welches die Teilchenenergie minimiert und die Streuung lokal maximiert. Je nach Anzahl der Teilchen und Moden gibt es eine Vielzahl solcher stabiler Teilchenkonfigurationen, die aber im Gegensatz zum Einzelmodenfall eine unterschiedliche, gestreute Gesamtintensität zur Folge haben.

Durch Rauschen, welches in realen, gedämpften Systemen immer präsent ist, können die Teilchen aber ihre Gleichgewichtsposition nach einiger Zeit wieder verlassen und finden dadurch stabilere Konfigurationen, in welchen mehr Licht gestreut wird. In dieser Weise passt sich das System an die vorherrschende Beleuchtung an und fungiert als adaptives Lichtsammelsystem. Auch wenn man zufällig zwischen einigen fix gewählten Beleuchtungen hin und her schaltet, steigt die gestreute Gesamtintensität langsam mit der Zeit an, weil sich die Teilchen nach und nach an alle verwendeten Beleuchtungen anpassen. Diesen Prozess kann man auch als „Lernen“ interpretieren: Das System hat Information über eine bestimmte Beleuchtung, die schon einmal oder öfters angewendet wurde, in der Konfiguration der Teilchen abgespeichert und kann somit besser auf diese reagieren. Die Funktionsweise ähnelt dabei der eines Hopfield-Netzes, welches ein einfaches Modell für das assoziative Gedächtnis ist.

Experimentell könnte so ein Aufbau sowohl mit kalten Gasen als auch mit Nano-Teilchen in Lösungen realisiert werden.

Abstract

Photons do not only carry energy but also momentum and thus they induce forces on material particles. Filling an optical Fabry-Pérot resonator with polarisable particles (e.g. atoms, molecules or nano-particles) and illuminating them with laser light from a direction transversal to the cavity axis, these forces give rise to a complex coupled dynamics. The particles scatter laser light into the resonator and thus create their own optical trap. In order to minimise their energy, they redistribute from a homogeneous to a crystalline particle order, whereby scattering is maximised while a deep optical potential is formed. Via losses through the mirrors the particles can dissipate kinetic energy ("cavity cooling"), which renders the ordered state stable. Using only one monochromatic laser beam, this self-organisation of polarisable particles in resonators is well understood and has already been experimentally demonstrated.

In this thesis we simulate the dynamical evolution of particles subject to simultaneous transversal illumination with many light colours (i.e. frequencies) which scatter into several resonator modes with distinct frequencies. Thereby the mode fields compete to push the particles into their respective preferred order, which ends in a stable equilibrium locally minimising the optical potential energy while locally maximising scattering. Using many particles and modes there exists a huge number of such stable particle configurations, which in contrast to the single-mode case result in differently strong total scattering.

Including noise, which is always present in real, damped systems, the particles might leave their equilibrium positions after some time and thus eventually find stabler configurations, which are associated with stronger scattering. This way the system adapts to the prevailing illumination and serves as an adaptive light collection system. Also when randomly switching between few fixed multi-colour illuminations, the total scattered intensity slowly increases with time as particles gradually improve their adaptation to all used illuminations. This process can also be interpreted as learning: The system has saved information about a certain already applied illumination in the configuration of the particles and can thus better react on reapplication. Moreover, it bears similarities to Hopfield networks, a simple model for associative memory.

Experimentally, such adaptive dynamics could be implemented in a wide range of systems from cold atoms and molecules to nano-particles in solutions.

Contents

Chapter 1.

Introduction

Laser light induces forces on polarisable particles (e.g. atoms, molecules and nanoparticles) and thus can be used to manipulate their motional degrees of freedom. When the laser is far detuned from any internal resonance and coherent scattering dominates over spontaneous emission, a standing wave in a free-space set-up creates a potential where the trap-depth is proportional to the local light intensity. Such optical lattices are used extensively for trapping and controlling cold and ultra-cold atoms [1].

As opposed to free space, in high-finesse optical resonators the back action of the particles onto the field is not negligible [2] leading to a coupled particle-field dynamics. This gives rise to a wealth of interesting effects including cavity cooling [3, 4], where the kinetic energy of the particles is dissipated via cavity losses.

Illuminating polarisable particles in a cavity from the side at sufficiently high intensity leads to a phase transition from homogeneous to crystalline particle order accompanied by super-radiant scattering [5, 6]. Via scattering into the cavity the particles create their own trapping potential and thus simultaneously minimise their energy and maximise scattering by redistributing into a Bragg-like ordered configuration. In a lossy cavity this self-ordering process is accompanied by a collective cooling mechanism, which is efficient even for high particle numbers [7–9], such that a stable configuration with constant scattering is attained in the long-time limit. As in such a system the particles adapt to varying frequencies and geometries of the illumination so that scattering into the cavity is maximised, it can be considered an adaptive light collection system.

In this thesis we extend the existing set-ups to many simultaneously applied laser pumps with various frequencies, each of which scatters into a specific mode and tries to push the particles into their ordered configuration. This leads to a multitude of stable ordered patterns with different scattering strength. Besides studying those stable configurations for few particles, we also numerically simulate the time evolution of many particles and modes for time-varying illuminations and under the influence of noise using a simplified classical model. This way the computational resources stay reasonably small even for many particles. Also, if the cavity resonances are sufficiently far apart, we can neglect cross-scattering and the computational resources only scale linearly with the

number of modes, which is in contrast to the full quantum mechanical case, where the limits of computability are already reached for only two modes and few particles [10].

Note that for cavities with many degenerate modes a complicated dynamics already occurs in the single frequency case [11, 12]. Interestingly, also in free space, self-ordering and spatial bunching have been observed and extensively studied [13, 14]. In this case, complicated dynamics have also been predicted for the multi-frequency case [15].

This thesis is organised as follows: First, we explain the basic physics involving light forces and single-frequency self-organisation in Chapter 2. We move on to the multi-frequency case in Chapter 3, where we specify the set-up and develop the theoretical model used throughout this thesis, which corresponds to the multi-frequency generalisation of the model used in e.g. [5]. That is, we start from a two-level atom and eliminate the internal atomic dynamics, such that we effectively end up with linearly polarisable particles. Hence, we will use the expressions atom and particle interchangeably throughout this thesis. In Chapter 4, we search for stable configurations using few particles and modes, which can still be graphically depicted. By means of visualisations we point out fundamental differences between single- and multi-colour laser pumps and qualitatively examine where the complicated potential landscape comes from. Finally, the time evolution for static multi-frequency illumination with noise and for time-varying illumination conditions is simulated in Chapter 5, where we observe adaptive behaviour which increases the scattered intensity with time.

The content of this thesis was recently published in Ref. [16].

Chapter 2.

Basic concepts

In this chapter we will introduce some basic physical concepts used in this thesis, whereby the interaction of atoms with light and the resulting mechanical forces form the basis.

2.1. Light forces

Let us first imagine a light beam with frequency ω which propagates through a cloud of atoms with resonance frequency ω_a. We observe two types of effects: On the one hand, the speed of propagation of light is modified by the presence of atoms, while on the other hand light is absorbed, attenuating the beam. These effects are called dispersive interactions, corresponding to an alteration of the real part of the refractive index with respect to free space, and dissipative interactions, originating from a non-zero imaginary part of the refractive index.

From the atoms' viewpoint, the interaction with photons leads to a shift of the atomic resonance $\omega = \omega_a$ by U_0 (ac-Stark shift), which is a dispersive effect, and a radiative broadening Γ_0 of the atomic ground state, which is a dissipative effect. Note that for an atom interacting with the vacuum field, the same effects are responsible for the Lamb shift and the natural linewidth of the excited state γ [17].

In a simple picture the interaction of light with atoms can be explained in terms of absorption and emission of photons by the atoms. Hereby stimulated emission corresponds to dispersive effects and spontaneous emission to dissipative effects. As photons carry momentum, absorption and emission of photons result in forces on atoms in light fields. There are two types of radiative forces acting on atoms, which can be categorised according to their origin: The dispersive *dipole force* and the dissipative *radiation pressure* [17].

In a propagating plane wave, an atom absorbs photons resulting in a recoil kick into the propagating direction. After a time specified by Γ_0, a further kick is exerted on the atom due to spontaneous emission into a random direction. To significantly exert a force many such cycles are necessary and thus the recoil kick stemming from the emission is averaged to zero, leading to a vanishing net force. So the only remaining force comes from the absorption and is directed into the propagating direction of the wave. This

dissipative force is called radiation pressure and is proportional to the phase gradient of the field and Γ_0. As stimulated emission compensates absorption in one cycle, it does not lead to a net force in the propagating wave set-up. But since this process occurs at a random time, it still leads to phase fluctuations. The velocity-dependence of the radiation pressure is the basic mechanism responsible for Doppler cooling [18] and magneto-optical traps [19].

In a standing plane wave photons are absorbed from both sides such that the radiation pressure vanishes, and spontaneous emission only leads to fluctuations proportional to Γ_0. However, interpreting the standing wave as two counter-propagating running waves, photons are redistributed between the two waves by stimulated emission. This leads to a momentum transfer of twice the photon momentum in one absorption-emission cycle and thus to a force proportional to the intensity gradient of the field, called dipole force. As the photon only changes momentum but retains its frequency, the dipole force is conservative. Thus a far-detuned standing wave creates a periodic potential known as optical lattice, which allows for flexibly simulating solid state systems like the Bose-Hubbard model [20].

2.2. Atoms in optical cavities

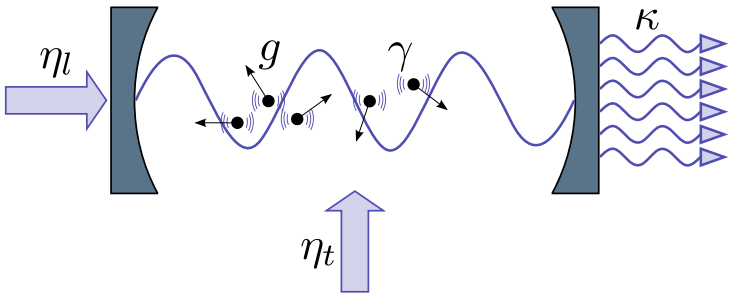

Figure 2.1.: Atoms with linewidth γ move in an optical resonator with cavity decay rate κ and interact with one cavity mode with a coupling constant g. In standard set-ups, the cavity is pumped longitudinally through one of the mirrors with the pump strength η_l. If the atoms are pumped transversally with a strength η_t, they scatter light into the cavity creating their own trapping field, which leads to self-ordering when η_t is above a certain threshold.

Placing particles in a high-finesse cavity significantly alters the mechanical effects of light leading to many phenomena not present in free space. This is mainly because particles and photons interact for several round trips resulting in a longer interaction time. Thus, in the strong coupling regime the back action of the particles on the light field is not negligible leading to coupled atom-field dynamics. The coupling of a two-level atom to a quantised field mode in the case of a lossless cavity is described by the well-known Jaynes-Cummings model [21].

In a realistic cavity however, light may leak out of the cavity with a decay rate κ, as depicted in Fig. 2.1. In standard set-ups, the resonator is driven by a laser with frequency ω and pump strength η_l through one of the mirrors. Inside of the cavity, two-level atoms couple to the cavity field with a coupling constant g and spontaneously decay with the rate γ.

A very useful phenomenon in such a set-up is cavity cooling [3], where kinetic energy of all particles is collectively reduced via the cavity dissipation channel characterised by the cavity linewidth κ. Here one exploits the time-delayed reaction of the cavity field (and thus the optical potential) on the particle motion, which for favourable parameter choices results in a friction force. But damping also leads to momentum diffusion, which in the optical domain at room temperature can be attributed to vacuum fluctuations of the cavity mode amplitude. In an alternative picture, the fluctuations can be traced back to the randomness of the photon loss through the two cavity mirrors. The competitive interplay of friction and diffusion finally leads to an equilibrium with a temperature close to $k_B T \approx \hbar\kappa$. One advantage with respect to direct laser cooling schemes where energy is dissipated via spontaneous emission (e.g. Doppler cooling) is that this limit can be well below the Doppler limit $k_B T \approx \hbar\gamma$. By not relying on spontaneous emission, reabsorption of photons can be avoided allowing for higher atomic gas densities. Note that we do not need to know the exact internal structure of the atom, making cavity cooling applicable to the broader range of polarisable particles, including molecules and nano-particles. However, the cooling time increases with the particle number, which results in limited scalability.

2.3. Self-organisation of atoms in a cavity

Now we slightly change the set-up: Instead of pumping through the mirrors along the cavity axis, we directly illuminate the atoms from the side of the cavity (i.e. from the transversal direction) with pump strength η_t (see Fig. 2.1), such that light is coherently scattered into the cavity via the atoms. Of course, the fields scattered by individual atoms interfere with each other. Each atom interacts with the collectively scattered interference field, leading to a mechanical force and thus atomic motion, which in turn changes the scattered field. This complex coupled dynamics creates a long range atom-atom interaction via the field and thus leads to a wealth of new phenomena. Particularly, above a certain threshold for the pump strength η_t the atoms self-organise into a crystalline pattern such that scattering into the cavity is maximised [5].

Let us have a closer look at this process with the help of Fig. 2.2, where the onset of self-organisation is depicted. We start with a homogeneously distributed atomic cloud in a high-Q optical cavity, which is transversally pumped by a red-detuned standing-wave laser with wavelength λ and wave number $k = 2\pi/\lambda$. For simplicity we assume plane waves and a sinusoidal mode function $f(x) = \sin(kx)$, where x is the direction along the cavity axis. The pump laser forms an optical potential in the transverse direction

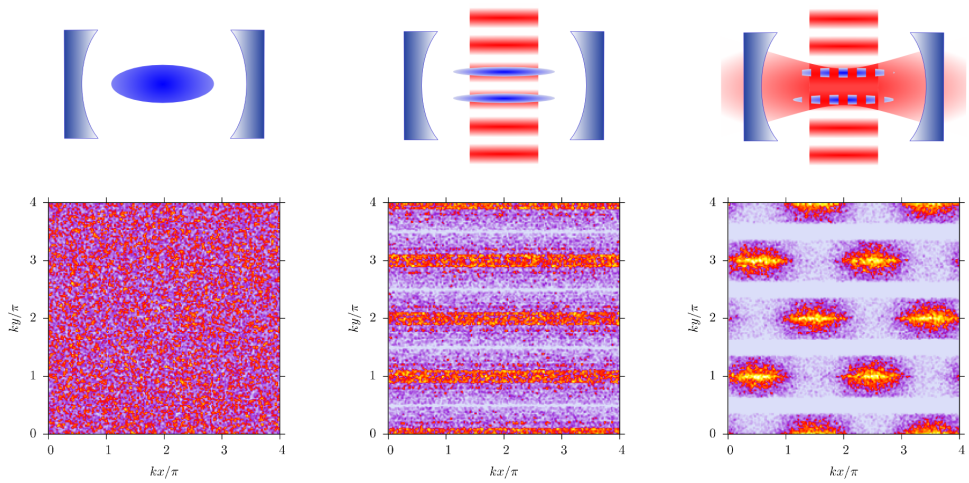

Figure 2.2.: The onset of a self-ordered pattern. Left: Homogeneously distributed atom cloud. Center: The standing wave laser creates an optical potential attracting the atoms to the anti-nodes of the field. Right: Atoms coherently scatter into the cavity and create their own potential in the longitudinal direction. If the pump intensity is above a threshold, they redistribute into one of two regular chequerboard patterns, maximising scattering into the cavity. The lower plots show a 2D-simulation using 50000 particles. This picture was adopted from [22].

and due to the red detuning the atoms move to the regions with high intensity, forming stripes separated by $\lambda/2$ (see center of Fig. 2.2).

Initially, no light is scattered since light which is coherently scattered by a homogeneously distributed atom ensemble destructively interferes. But as we have a finite particle number, density fluctuations lead to the buildup of a small scattered field in the cavity, which gives rise to a small dipole force towards the anti-nodes (i.e. intensity maxima at $kx = \pi/2 + l\pi$ with some integer l) of this field acting on the particles. As more and more particles tend to be closer to the anti-nodes, more light is scattered enhancing this tendency and finally resulting in a runaway effect. Yet there is one problem: Since the anti-nodes of the cavity field are separated by $\lambda/2$, light scattered from adjacent anti-nodes destructively interferes. However, it turns out that the atoms randomly choose a specific pattern gathering at anti-nodes with either even or odd l such that $\sin(kx)$ is either close to 1 or -1. The atom clouds are now separated by λ and thus coherently scattered light constructively interferes, which gives rise to a quadratical increase of scattered intensity with the particle number, an effect called superradiance. Due to interference of cavity field and pump field, the particles redistribute according to one of the two equivalent chequerboard patterns (see right picture in Fig. 2.2), as neighbouring stripes in the transversal direction have opposite phase. Thus the phase of the output field of the cavity produced by the two distinct patterns differs by π. This measurable

phase relation has been used to prove the effect experimentally in [6].

The system also comprises an efficient cooling effect necessary for stabilisation of the self-ordering process. As in standard cavity cooling schemes [3], the temperature limit is proportional to κ, however, in the current system the cooling efficiency does not depend on the particle number [5, 7]. In a more general model, scattering into several modes is considered [2].

In this thesis we will examine an "upgrade" of the system described above: Instead of transversally pumping with only one single frequency, we consider several laser pumps with different frequencies, where each is scattered into one specific cavity mode with similar frequency. Using parameters where self-organisation is energetically favourable, the atoms will try to organise according to the cavity field. If the mode frequencies are far apart, we can neglect interference between the individual cavity mode fields and add up their intensities, which are proportional to $\sin^2(nkx)$ for the n-th mode. However, generally the maxima of the intensities of each mode field do not coincide and so the different fields compete to push the atoms to their maxima. From the atoms' point of view, this results in a complicated potential landscape with many local minima of different depth, where the precise shape of the optical potential mainly depends on which modes are pumped. This leads to a wealth of phenomena beyond single-frequency self-organisation, a few of which will be explored in the course of this work.

Chapter 3.

Model

Here we will introduce the mathematical model describing the physical system used in this thesis. For this we will start with two-level atoms and quantised fields obeying a quantum master equation. In the course of the derivation, we will first adiabatically eliminate the inner degrees of freedom of the atoms, rendering the two-level atoms polarisable quantum particles. Thereafter we will perform a semi-classical approximation for both, fields and particles, such that we end up with a set of coupled stochastic differential equations [23], which are not only valid for atoms in a certain regime, but for polarisable, interaction-free, point-like particles in general. This comprises atoms, molecules and nano-particles. One could also derive the equations without quantum noise by starting from the completely classical model of a point-like dipole, as in [24].

3.1. Set-up

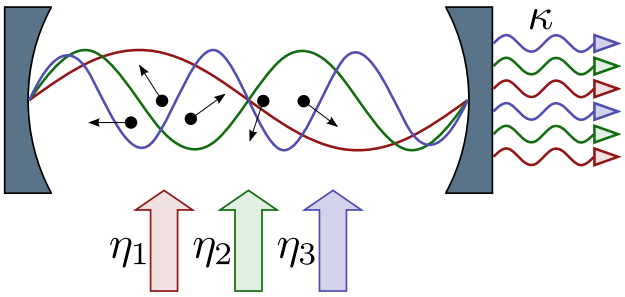

Figure 3.1.: Scheme of particle ensemble moving inside a lossy optical resonator characterised by the decay rate κ illuminated by laser beams with various frequencies and pump strengths η_1, η_2 and η_3.

We consider N identical two-level atoms of mass m with resonance frequency ω_a and linewidth γ in a standing-wave optical resonator supporting a large number of modes of similar finesse with wave numbers $k_n := nk$ ($n \in \mathbb{N}$) and corresponding frequencies

$\omega_n := ck_n$, where k is the wave number of a chosen base mode and c is the speed of light in vacuum. For simplicity, we restrict ourselves to one dimension x along the cavity axis and consider the normalised mode functions $f_n(x) = \sin(k_n x)$, as depicted in Fig. 3.1. The resonator is lossy with a cavity linewidth κ_n, which is frequency-dependent in general. The atoms are transversally illuminated by lasers with frequencies $\omega_{p,n}$, each of which is close to a specific mode frequency $\omega_{c,n}$, but far detuned from the atomic frequency such that the atoms stay in their ground state $|g\rangle$ with high probability. Thus we can neglect spontaneous emission and adiabatically eliminate the excited state $|e\rangle$. This way, the atoms coherently scatter pump light by a specific laser, whose amplitude and phase depend on the position of the atoms, into its corresponding cavity mode.

3.2. Master equation

Describing such an open quantum mechanical system in principle requires to solve the master equation for the density matrix $\rho(t)$ describing the state of the system. It can be written as

$$\dot{\rho} = -\frac{i}{\hbar}[H, \rho] + \mathcal{L}\rho, \tag{3.1}$$

where the Liouvillian damping operator

$$\mathcal{L}\rho := \sum_n \kappa_n (2a_n \rho a_n^\dagger - a_n^\dagger a_n \rho - \rho a_n^\dagger a_n) \tag{3.2}$$

includes the dissipative effects. As spontaneous emission is neglected, only the cavity loss with the rate $2\kappa_n$ contributes. Here a_n and $a_n^\dagger$ denote the bosonic creation and annihilation operators of a photon in the n-th mode, respectively.

3.2.1. Hamiltonian in the dipole approximation

The coherent dynamics are given by the Hamiltonian of the system, which comprises the kinetic and potential energy of the atoms, the potential energy of the cavity mode fields, and the interaction between atoms and field in the dipole approximation (e.g. [25])

$$H_D = \sum_j \frac{p_j}{2m} + \hbar\omega_a \sum_j \sigma_j^\dagger \sigma_j + \hbar \sum_n \omega_{c,n} a_n^\dagger a_n - \sum_j \hat{d}_j \hat{E}(x_j), \tag{3.3}$$

where x_j and p_j are the position and momentum operators of the center-of-mass (CM) motion of the j-th atom, respectively. The internal atomic degrees of freedom are taken account of by the lowering operator $\sigma_j := |e\rangle_j \langle g|$ and the raising operator $\sigma_j^\dagger := |g\rangle_j \langle e|$.

The latter two are used to express the dipole moment operator as $\hat{d}_j = d\hat{x}_{rel,j} = d(\sigma_j + \sigma_j^\dagger)$, where d is the transition dipole moment. The electric field operator is

composed of the classical pump field with complex amplitudes $\mathcal{E}_n$ and the quantised cavity field, namely

$$\hat{E}(x) = E_{pump}(t) + \hat{E}_{cav}(x,t) = i\sum_n \left(\mathcal{E}_n e^{-i\omega_{p,n}t} - \mathcal{E}_n^* e^{i\omega_{p,n}t}\right) + i\sum_n \sqrt{\frac{\hbar\omega_{c,n}}{2\epsilon_0\mathcal{V}}} f_n(x)(a_n - a_n^\dagger), \tag{3.4}$$

where the square root is the field created by a single photon, $\mathcal{V}$ is the mode volume and ϵ_0 is the vacuum permittivity. Thereby we assume that the pump field is constant along the x-direction, which is a good approximation if the region of interest is in the center of a wide laser beam.

3.2.2. Rotating wave approximation

Inserting the field back into the Hamiltonian, we encounter terms oscillating with different frequencies:

- $a_n\sigma_j^\dagger$ and $a_n^\dagger\sigma_j$ are oscillating with $|\omega_{c,n} - \omega_a|$.
  $\mathcal{E}_n e^{-i\omega_{p,n}t}\sigma_j^\dagger$ and $\mathcal{E}_n^* e^{i\omega_{p,n}t}\sigma_j$ are oscillating with $|\omega_{p,n} - \omega_a|$.
- $a_n\sigma_j$ and $a_n^\dagger\sigma_j^\dagger$ are oscillating with $|\omega_{c,n} + \omega_a|$.
  $\mathcal{E}_n e^{-i\omega_{p,n}t}\sigma_j$ and $\mathcal{E}_n^* e^{i\omega_{p,n}t}\sigma_j^\dagger$ are oscillating with $|\omega_{p,n} + \omega_a|$.

We assume that $|\omega_{c,n} - \omega_a|, |\omega_{p,n} - \omega_a| \ll \omega_a$, such that $\omega_a \approx \omega_{c,n} \approx \omega_{p,n}$. In this case, the terms evolving with the sum of two frequencies are fast rotating compared to the terms evolving with the difference and will almost average to zero. Thus we neglect[1] those terms, which is commonly known as the *rotating wave approximation* (RWA) [26].

The interaction term in the rotating wave approximation reads

$$\hat{d}_j\hat{E} = i\hbar\sum_n \left(\tilde{\eta}_n e^{-i\omega_{p,n}t}\sigma_j^\dagger - \tilde{\eta}_n^* e^{i\omega_{p,n}t}\sigma_j\right) + i\hbar\sum_n \mathcal{G}_n(x_j)\left(a_n\sigma_j^\dagger - \sigma_j a_n^\dagger\right), \tag{3.5}$$

with the laser Rabi frequency $\tilde{\eta}_n := d\mathcal{E}_n/\hbar$ and a position-dependent coupling $\mathcal{G}_n(x) := g_n f_n(x)$, containing the single photon Rabi frequency $g_n := d\sqrt{\hbar\omega_{c,n}/(2\epsilon_0\mathcal{V})}/\hbar$.

3.2.3. Rotating frame

In order to get rid of the explicit time dependence originating from the large optical frequencies, we would like to consider the system in a rotating frame of reference. As there is one specific pump frequency $\omega_{p,n}$ close to every mode frequency $\omega_{c,n}$, we use a frame rotating with $\omega_{p,n}$ for the n-th mode field, leading to the detunings $\delta_{c,n} := \omega_{p,n} - \omega_{c,n}$ (see Fig. 3.2). For the internal atomic degrees of freedom, though, there is not only a single

[1] We additionally need to assume that the Rabi frequencies are much smaller than the atomic resonance, hence $|\tilde{\eta}_n|, g_n \ll \omega_a \approx \omega_{c,n} \approx \omega_{p,n}$.

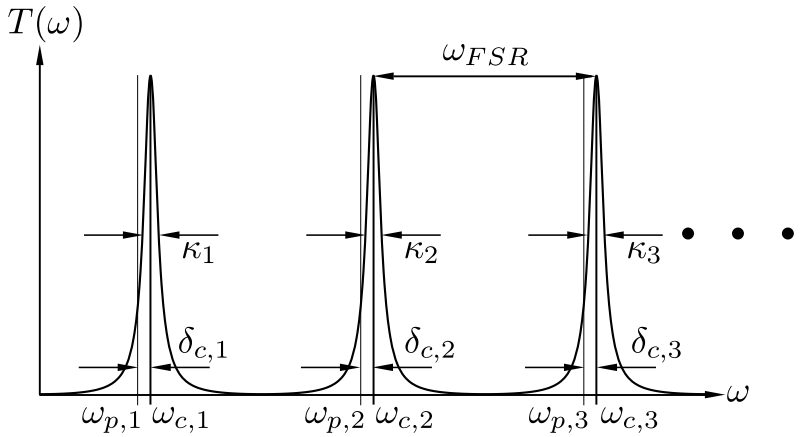

Figure 3.2.: Transmission spectrum of a standing-wave optical resonator with the free spectral range ω_{FSR}. Each pump frequency $\omega_{p,n}$ is close to a specific cavity resonance peak at $\omega_{c,n}$ ($|\delta_{c,n}| \ll \omega_{FSR}$), which requires that the peaks are sufficiently distinct ($\kappa_n \ll \omega_{FSR}$).

corresponding pump frequency as the atoms feel all pump frequencies. However, this is not problematic if we assume that all cavity frequencies $\omega_{c,n}$ (and pump frequencies $\omega_{p,n}$) are far away from the atomic resonance, such that the atom cannot distinguish between them. Under this assumption it makes sense to introduce a frequency Ω, which is chosen among the pump frequencies (e.g. the lowest one, $\Omega \equiv \omega_{p,1}$ as in Fig. 3.3), since its deviation from the actual pump frequencies $\Delta_n := \omega_{p,n} - \Omega$ is small compared to the atomic detuning $\delta_a := \Omega - \omega_a$ for all n. This also implies that $|\delta_a| \gg \Delta\omega_c$, where $\Delta\omega_c$ is the spread of the cavity resonance frequencies (see Fig. 3.3).

By substituting the operators in the Hamiltonian by

$$\sigma_j \to \sigma_j e^{-i\Omega t} \qquad a_n \to a_n e^{-i\omega_{p,n}t}, \tag{3.6}$$

and taking the product rule of differentiation into account[2], we obtain the Hamiltonian in a rotating frame

$$\begin{aligned} H_{RF} = \sum_j \frac{p_j}{2m} - \hbar\delta_a \sum_j \sigma_j^\dagger \sigma_j - \hbar \sum_n \delta_{c,n} a_n^\dagger a_n - i\hbar \sum_{n,j} \left(\tilde{\eta}_n e^{-i\Delta_n t} \sigma_j^\dagger - \tilde{\eta}_n^* e^{i\Delta_n t} \sigma_j \right) - \\ - i\hbar \sum_{n,j} \mathcal{G}_n(x_j) \left(\sigma_j^\dagger a_n e^{-i\Delta_n t} - a_n^\dagger \sigma_j e^{i\Delta_n t} \right). \end{aligned} \tag{3.7}$$

Still, H_{RF} has an explicit time-dependence because of the deviation of Ω from an arbitrary pump frequency Δ_n.

[2]Formally, this rotation amounts to applying the unitary operator $U(t) = \exp(it(\sum_n \omega_{p,n} a_n^\dagger a_n + \Omega \sum_j \sigma_j^\dagger \sigma_j))$. The new Hamiltonian in the rotating frame is then given by $H_{RF} = UHU^\dagger + i\hbar \dot{U} U^\dagger$.

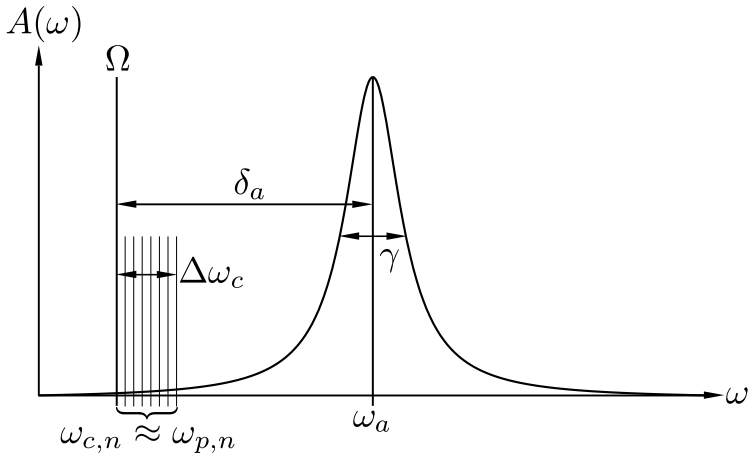

Figure 3.3.: Absorption spectrum of a radiating atomic dipole compared with the cavity resonances. In our model $|\delta_a|$ is much larger than the spread of the cavity resonance frequencies $\Delta\omega_c$, which implies that all $\omega_{c,n}$'s can be summarised by one close-by frequency Ω as they are the same from the atom's viewpoint. Assuming that $|\delta_a|$ is much larger than the atomic linewidth γ leads to negligible excitation of the atom.

3.2.4. Effective Hamiltonian

In the low saturation regime ($|\delta_a| \gg \gamma$), we can adiabatically eliminate the internal degrees of freedom of the atom. For this, we rewrite the Hamiltonian in terms of the operator

$$\tilde{\sigma}_{j,n} := \sigma_j e^{i\Delta_n t} \tag{3.8}$$

which evolves on the time scale of $\delta_a + \Delta_n$. The Heisenberg equation for this operator is non-linear and reads

$$\dot{\tilde{\sigma}}_{j,n} = \frac{i}{\hbar}[H, \tilde{\sigma}_{j,n}] = i\delta_a\tilde{\sigma}_{j,n} + \sum_m \left(\mathcal{G}_m(x_j)a_m + \tilde{\eta}_m\right)\sigma_j^z e^{i(\omega_{p,n}-\omega_{p,m})t}, \tag{3.9}$$

where we used the commutation relations

$$[\tilde{\sigma}_{l,n}^\dagger, \tilde{\sigma}_{j,m}] = \delta_{lj}\sigma_j^z e^{i(\Delta_m-\Delta_n)t} = \delta_{lj}\sigma_j^z e^{i(\omega_{p,m}-\omega_{p,n})t} \qquad [\tilde{\sigma}_{l,n}, \tilde{\sigma}_{j,m}^\dagger\tilde{\sigma}_{j,m}] = \delta_{lj}\tilde{\sigma}_{j,n}. \tag{3.10}$$

As almost the whole population is in the ground state, we substitute the inversion by a c-number $\sigma_j^z = -1$, rendering the equation linear. This substitution is sometimes called *bosonisation* since the two-level atom is considered an infinite ladder like a bosonic mode [2].

Also, as $|\delta_a + \Delta_n| \approx |\delta_a| \gg |\delta_{c,n}|$ the operator $\tilde{\sigma}_{j,n}$ evolves much faster than the field operators a_n. Hence we can assume that they instantaneously adapt to a changing field ($\dot{\tilde{\sigma}}_{j,n} = 0$), yielding

$$\tilde{\sigma}_{j,n} = \frac{1}{i\delta_a}\sum_m (\mathcal{G}_m(x_j)a_m + \tilde{\eta}_m)e^{i(\omega_{p,n}-\omega_{p,m})t}. \tag{3.11}$$

Putting this back into the Hamiltonian gives rise to cross-scattering interference terms containing $e^{\pm i(\omega_{p,n}-\omega_{p,m})t}$, which oscillate with the pump frequency differences. For $n \neq m$ these terms almost average to zero as their oscillation is much faster than the response time of the atomic motion and the oscillation of the field terms, that is $|\delta_{c,n}| \ll \omega_{FSR} := \omega_{c,n+1} - \omega_{c,n} \lesssim |\omega_{p,n} - \omega_{p,m}|$ (see Fig. 3.2). Thus we can neglect[3] those cross-scattering, fast-rotating terms and finally obtain the *effective Hamiltonian*

$$H = \sum_j \frac{p_j^2}{2m} + \hbar \sum_n \left[-\left(\delta_{c,n} - U_{0,n} \sum_j \sin^2(k_n x_j) \right) a_n^\dagger a_n + \eta_n \sum_j \sin(k_n x_j)(a_n + a_n^\dagger) \right] \tag{3.12}$$

with the effective pump strength $\eta_n := g_n \tilde{\eta}_n / \delta_a$ and the light shift per photon $U_{0,n} := g_n^2/\delta_a$.

With (3.1), this yields an effective master equation describing the coupled center-of-mass and field quantum dynamics. Since the internal atomic dynamics have been eliminated, the atoms act as a medium with a refractive index resulting in position-dependent shifts $U_{0,n} \sum_j \sin^2(k_n x_j)$ of the bare cavity resonances $\delta_{c,n} = 0$. In addition to that, we obtain the usual pump term for longitudinal pumping (see e.g. [3]) but with a pump strength $\eta_n \sum_j \sin(k_n x_j)$ depending on the atom positions. A very similar Hamiltonian for the single-frequency case which could be intuitively generalised to (3.12) has been used in [2, 7, 27].

We conclude this section with a summary of the assumptions made during the derivation of the effective Hamiltonian:

$$|\delta_a| \gg \gamma, \tag{3.13a}$$

$$|\delta_a| \gg \Delta\omega_c \gtrsim |\Delta_n| \quad \forall\, n, \tag{3.13b}$$

$$|\delta_{c,n}| \ll \omega_{FSR} \lesssim |\omega_{p,n} - \omega_{p,m}| \quad \forall\, n \neq m. \tag{3.13c}$$

3.3. Semi-classical treatment

Employing the phase space representation of quantum mechanics, we formulate the operator-based master equation in the language of statistical mechanics. As opposed to the classical case, for a quantum system the distribution functions do not fulfil all properties of a genuine probability distribution, particularly they may take on negative values. Hence they are called *quasi-probability distributions*.

Due to the similarity to classical theories, this is the appropriate formalism to compare our system to the classical limit and conduct semi-classical approximations. In this vein, we transform our high-dimensional master equation to a partial differential equation (PDE) for the Wigner function, a quasi-probability distribution. After that we systematically

[3] To justify this we further need to fulfil the condition for the Rabi frequencies $|U_{0,n}|, |\eta_n| \ll \omega_{FSR}$, as in the RWA above.

truncate the order of the PDE to obtain a Fokker-Planck equation, which can be reformulated as a set of coupled stochastic differential equations (SDE). The SDEs can be easily interpreted and solved numerically.

3.3.1. Wigner phase space distribution

The Wigner phase space distribution of a quantum state described by a density operator ρ is given by [28]

$$W(x,p) = \frac{1}{2\pi\hbar}\int_{-\infty}^{\infty} \mathrm{d}\xi\, \exp\left(-\frac{i}{\hbar}p\xi\right)\left\langle x+\frac{1}{2}\xi\right|\rho\left|x-\frac{1}{2}\xi\right\rangle, \tag{3.14}$$

where x and p are c-numbers and not operators. The distribution can be generalised to a combined Wigner function $W(x,p,\alpha,\alpha^*)$ of CM motion and field, where we consider both, atoms and field in phase space [23]. To rewrite the master equation in terms of this quasi-probability distribution, we use the operator correspondences [29]

$$x\rho \leftrightarrow \left(x+\frac{i\hbar}{2}\frac{\partial}{\partial p}\right)W(x,p) \qquad \rho x \leftrightarrow \left(x-\frac{i\hbar}{2}\frac{\partial}{\partial p}\right)W(x,p) \tag{3.15a}$$

$$p\rho \leftrightarrow \left(p-\frac{i\hbar}{2}\frac{\partial}{\partial x}\right)W(x,p) \qquad \rho p \leftrightarrow \left(p+\frac{i\hbar}{2}\frac{\partial}{\partial x}\right)W(x,p) \tag{3.15b}$$

$$a\rho \leftrightarrow \left(\alpha+\frac{1}{2}\frac{\partial}{\partial \alpha^*}\right)W(\alpha,\alpha^*) \qquad \rho a^\dagger \leftrightarrow \left(\alpha^*+\frac{1}{2}\frac{\partial}{\partial \alpha}\right)W(\alpha,\alpha^*) \tag{3.15c}$$

$$a^\dagger\rho \leftrightarrow \left(\alpha^*-\frac{1}{2}\frac{\partial}{\partial \alpha}\right)W(\alpha,\alpha^*) \qquad \rho a \leftrightarrow \left(\alpha-\frac{1}{2}\frac{\partial}{\partial \alpha^*}\right)W(\alpha,\alpha^*). \tag{3.15d}$$

In the course of the derivation we encounter commutator and anti-commutator of functions $g(x)$ of the position operator x

$$[g(x),\rho] \leftrightarrow \sum_{l\in 2\mathbb{N}+1}\frac{2}{l!}\frac{\partial^l g(x)}{\partial x^l}\left(\frac{i\hbar}{2}\right)^l\frac{\partial^l}{\partial p^l}W(x,p) \tag{3.16a}$$

$$\{g(x),\rho\} \leftrightarrow \sum_{l\in 2\mathbb{N}}\frac{2}{l!}\frac{\partial^l g(x)}{\partial x^l}\left(\frac{i\hbar}{2}\right)^l\frac{\partial^l}{\partial p^l}W(x,p), \tag{3.16b}$$

which are derived in Appendix A.

As our master equation contains functions of operators, whose derivatives do not vanish, the resulting PDE contains infinite expansions with high-order derivatives of W. In the following we will motivate some approximations which allow us to truncate those expansions, finally yielding a Fokker-Planck equation, only containing derivatives up to second order.

3.3.2. Fokker-Planck equation

Our master equation contains the functions $g(x_j) = \sin(k_n x_j)$ or $g(x_j) = \sin^2(k_n x_j)$ for which we obtain $\partial^l g(x_j)/\partial x_j^l \sim k_n^l$. Moreover, for the width Δp of a Gaussian-like distribution function $W(p)$ the following relations hold

$$\left|\max\frac{\partial W}{\partial p}\right| \sim \frac{1}{\Delta p} \Rightarrow \left|\frac{\partial W}{\partial p}\right| \lesssim \frac{1}{\Delta p}. \tag{3.17}$$

Hence, if $\hbar k_n/\Delta p \ll 1$ only the first terms in the expansion (3.16) contribute significantly, which justifies truncating the expansion at first order to avoid third-order terms in the PDE, taking also field derivatives into account. Within this approximation we can use

$$[g(x), \rho] \leftrightarrow i\hbar \frac{\partial g}{\partial x}\frac{\partial}{\partial p} W(x,p) \tag{3.18a}$$

$$\{g(x), \rho\} \leftrightarrow 2g(x) W(x,p). \tag{3.18b}$$

Physically, the condition $\hbar k_n/\Delta p \ll 1$ means that width of the momentum distribution Δp should not be altered significantly upon emission or absorption of a photon associated with a recoil kick $\hbar k_n$ [23]. We can reformulate this condition in terms of the temperature T associated with Δp and the recoil energy E_R [2] as

$$k_B T \gg E_{R,n} := \frac{\hbar^2 k_n^2}{2m} = n^2 \frac{\hbar^2 k^2}{2m} = n^2 E_R. \tag{3.19}$$

This is the semi-classical approximation of the CM motion of the particles, requiring that the atom ensemble is not too cold such that the wave packets of the particles are small compared to the optical wavelength.

There is a further assumption regarding the field. To avoid the third order derivative in the $U_{0,n}$-term

$$\left(|\alpha_n|^2 - \frac{1}{2} - \frac{1}{4}\frac{\partial^2}{\partial\alpha_n \partial\alpha_n^*}\right)\frac{\partial}{\partial p_j} W \tag{3.20}$$

we have to neglect the second-order derivative $\partial^2/\partial\alpha_n\partial\alpha_n^*$ compared to $|\alpha_n|^2$. A sufficient condition is to consider fields close to coherent states with photon numbers much larger than 1 [23]. Consequently, we can also neglect $1/2$ over $|\alpha_n|^2$. In this step, the semi-classical approximation of the cavity fields was made.

Under these assumptions, we obtain a Fokker-Planck equation for the combined Wigner

function $W(x_1, ...x_N, p_1, ..., p_N, \alpha_1, ..., \alpha_M, \alpha_1^*, ..., \alpha_M^*)$

$$\begin{aligned}\frac{\mathrm{d}}{\mathrm{d}t}W = \Bigg[& i\sum_n \left(U_{0,n}\sum_j \sin^2(k_n x_j) - \delta_{c,n}\right)\left(\frac{\partial}{\partial\alpha_n}\alpha_n - \frac{\partial}{\partial\alpha_n^*}\alpha_n^*\right) \\ & + i\sum_{n,j}\eta_n \sin(k_n x_j)\left(\frac{\partial}{\partial\alpha_n} - \frac{\partial}{\partial\alpha_n^*}\right) \\ & + \hbar\sum_{n,j} k_n\left(U_{0,n}|\alpha_n|^2\sin(2k_n x_j) + \eta_n\cos(k_n x_j)(\alpha_n + \alpha_n^*)\right)\frac{\partial}{\partial p_j} \\ & - \sum_j \frac{p_j}{m}\frac{\partial}{\partial x_j} \\ & + \sum_n \kappa_n\left(\frac{\partial}{\partial\alpha_n}\alpha_n + \frac{\partial}{\partial\alpha_n^*}\alpha_n^* + \frac{\partial^2}{\partial\alpha_n\partial\alpha_n^*}\right)\Bigg] W.\end{aligned} \tag{3.21}$$

3.3.3. Stochastic differential equations

This Fokker-Planck equation can be transformed into a set of stochastic differential equations for the stochastic variables with the distribution W (summarised by the vector $\boldsymbol{X} = (x_1, \ldots, x_N, p_1, \ldots, p_N, \alpha_1, \ldots, \alpha_M)^{\mathrm{T}}$) of the form

$$\mathrm{d}\boldsymbol{X} = \boldsymbol{A}(\boldsymbol{X}, t)\mathrm{d}t + \boldsymbol{B}(\boldsymbol{X}, t)\mathrm{d}\boldsymbol{W}, \tag{3.22}$$

where $\mathrm{d}\boldsymbol{W}$ is a $L := (2N + M)$-dimensional Wiener process. $\boldsymbol{A}$ and $\boldsymbol{B}$ have to be determined from the FPE using the correspondence [30]

$$\frac{\partial f(\boldsymbol{x}, t)}{\partial t} = -\sum_{i=1}^{L}\frac{\partial}{\partial x_i}[A_i(\boldsymbol{x}, t)f(\boldsymbol{x}, t)] + \frac{1}{2}\sum_{i=1}^{L}\sum_{j=1}^{L}\frac{\partial^2}{\partial x_i\partial x_j}[D_{ij}(\boldsymbol{x}, t)f(\boldsymbol{x}, t)], \tag{3.23}$$

where $\boldsymbol{A}$ is the drift vector and

$$D_{ij}(\boldsymbol{x}, t) = \sum_k B_{ik}B_{jk} = [\boldsymbol{B}\boldsymbol{B}^{\mathrm{T}}]_{ij} \tag{3.24}$$

is the diffusion matrix.

Applying this to our Fokker-Planck equation (3.21) yields the coupled stochastic differential equations

$$\mathrm{d}x_j = \frac{p_j}{m}\mathrm{d}t \tag{3.25a}$$

$$\mathrm{d}p_j = -\hbar\sum_n k_n\left(U_{0,n}|\alpha_n|^2\sin(2k_n x_j) + \eta_n(\alpha_n + \alpha_n^*)\cos(k_n x_j)\right)\mathrm{d}t \tag{3.25b}$$

$$\begin{aligned}\mathrm{d}\alpha_n = i\left(\delta_{c,n} - U_{0,n}\sum_j \sin^2(k_n x_j)\right)\alpha_n\mathrm{d}t - \kappa_n\alpha_n\mathrm{d}t - i\eta_n\sum_j \sin(k_n x_j)\mathrm{d}t + \\ + \sqrt{\frac{\kappa_n}{2}}(\mathrm{d}W_{1,n} + i\mathrm{d}W_{2,n}).\end{aligned} \tag{3.25c}$$

The noise only affects the field, as cavity loss is the only dissipation channel. If we had included spontaneous emission, also the momentum equation would have a noise term.

3.4. Classical treatment

Since we are interested in qualitative effects for multi-color pump lasers, we will deal with classical particles throughout this thesis by using the equations (3.25) without the field noise. Moreover, we will neglect the n-dependence of κ_n, $\delta_{c,n}$ and $U_{0,n}$. For κ this simply means that the loss rate of the mirrors is constant over the used frequency range, while for δ_c this choice is technically reasonable when implementing the laser beams with standard comb technology. As all cavity frequencies are far detuned from the atomic resonance and $\omega_{FSR} \ll \omega_{c,n}$ also the frequency dependence of $U_{0,n} \propto \omega_{c,n}/\delta_a$ can be neglected. This way we get a set of coupled non-linear differential equations

$$\dot{x}_j = \frac{p_j}{m}, \tag{3.26a}$$

$$\dot{p}_j = -\hbar \sum_n k_n \left(U_0 |\alpha_n|^2 \sin(2k_n x_j) + \eta_n (\alpha_n + \alpha_n^*) \cos(k_n x_j) \right) \tag{3.26b}$$

$$\dot{\alpha}_n = i \left(\delta_c - U_0 \sum_j \sin^2(k_n x_j) \right) \alpha_n - \kappa \alpha_n - i \eta_n \sum_j \sin(k_n x_j). \tag{3.26c}$$

The force on the j-th particle

$$F_j(x_j, \alpha_1, ..., \alpha_M) = -\hbar \sum_n k_n \left(U_0 |\alpha_n|^2 \sin(2k_n x_j) + \eta_n (\alpha_n + \alpha_n^*) \cos(k_n x_j) \right) \tag{3.27}$$

as given in (3.26b) depends on the position and all fields, which are dynamical variables themselves. The term proportional to U_0 has a periodicity of $\lambda/2$, while the other term proportional to η_n is λ-periodic. The sign of $\alpha_n + \alpha_n^* = 2\Re(\alpha_n)$ determines which of the two equivalent self-organised patterns is formed.

3.5. Bad cavity limit

In the bad cavity limit [27], where the cavity modes decay fast on the timescale of the atomic motion ($\kappa \gg \omega_R := \hbar k^2/(2m)$), it can be assumed that the fields are always in their steady state $\dot{\alpha}_n = 0$ and thus react instantaneously to a changing atom configuration. From (3.26c) we obtain

$$\alpha_n(x_1, ..., x_N) = \eta_n \frac{\sum_j \sin(k_n x_j)}{\delta_c - U_0 \sum_j \sin^2(k_n x_j) + i\kappa}. \tag{3.28}$$

The force (3.27) now solely depends on all particle positions $F_j = F_j(x_1, ..., x_N)$.

3.6. Over-damped motion

Although cavity cooling and thus friction is already included in the coupled equations (3.26), we can alternatively add a large additional friction term to avoid the search for suitable parameter ranges, which is not necessary for the demonstration of the qualitative effect. The momentum equation (3.26b) with external damping thus gets

$$\dot{p}_j = F_j - \mu p_j, \tag{3.29}$$

with the external damping rate μ. For large damping, we can neglect $\dot{p_j}$ compared to the other terms. With (3.29) and (3.26a) we obtain the equation of motion for the *over-damped case*

$$\dot{x}_j = \frac{F_j}{\mu}, \tag{3.30}$$

where the velocity is proportional to the force. Hence, particles stop as soon as they find a stable point and do not oscillate around them. This is very practical if we just want to find stable points.

3.7. Stability criterion

At an *equilibrium point* the force on every particle has to be zero, which in the bad cavity limit yields N non-linear equations

$$F_i(x_1, ..., x_N) \stackrel{!}{=} 0 \qquad \forall i. \tag{3.31}$$

The solutions of this equation are candidates for stable points.

Now one might be tempted to introduce a collective potential $V(x_1, ..., x_N)$ such that $F_i = -\partial V/\partial x_i$, and determine minima and maxima (and thus stability) by analysing the definiteness of the Hessian matrix of the potential. However, it turns out that such a potential does not exist in general [27]. That is because in general we obtain $\partial F_i/\partial x_j \neq \partial F_j/\partial x_i$ implying that $\partial^2 V/\partial x_i \partial x_j \neq \partial^2 V/\partial x_j \partial x_i$, which contradicts Young's theorem. Note that this behaviour is not surprising as we deal with an open, non-conservative system, where the lasers pump energy into the system while energy is lost through the mirrors.

Instead, we consider the asymptotic stability of the dynamic over-damped system [31]. As stated before, in the over-damped case the velocity of each particle is simply proportional to the force on this particle

$$\dot{\boldsymbol{x}} = \tilde{\boldsymbol{F}}(\boldsymbol{x}) \propto \boldsymbol{F}(\boldsymbol{x}) \tag{3.32}$$

where $\boldsymbol{x} = (x_1, ..., x_N)^T$ and $\boldsymbol{F}(\boldsymbol{x}) = (F_1(\boldsymbol{x}), ..., F_N(\boldsymbol{x}))^T$. The force can be linearised around an equilibrium point $\boldsymbol{x_e}$ which yields a differential equation

$$\dot{\boldsymbol{x}} = \underbrace{\tilde{\boldsymbol{F}}(\boldsymbol{x_e})}_{=0} + \mathcal{J}_{\tilde{\boldsymbol{F}}}(\boldsymbol{x_e})(\boldsymbol{x} - \boldsymbol{x_e}) = \mathcal{J}_{\tilde{\boldsymbol{F}}}(\boldsymbol{x_e})(\boldsymbol{x} - \boldsymbol{x_e}), \tag{3.33}$$

where $\mathcal{J}_{\tilde{\boldsymbol{F}}}$ is the Jacobian matrix of $\tilde{\boldsymbol{F}}$. For the variable $\boldsymbol{\delta x} = \boldsymbol{x} - \boldsymbol{x_e}$ we get the linear system

$$\dot{\boldsymbol{\delta x}} = \mathcal{J}_{\tilde{\boldsymbol{F}}}(\boldsymbol{x_e})\boldsymbol{\delta x} \tag{3.34}$$

which is *globally asymptotically stable* if and only if $\Re\lambda_i(\mathcal{J}_{\tilde{\boldsymbol{F}}}) < 0$ where $\lambda_i(A)$ are the eigenvalues of A. As only the sign of the eigenvalues is important we can translate the criterion to $\Re\lambda_i(\mathcal{J}_{\boldsymbol{F}}) < 0$ for all i.

If the linearised system is stable (i.e. the above criterion is fulfilled) then the nonlinear system is *locally asymptotically stable*. On the other hand, if for some i, $\Re\lambda_i(\mathcal{J}_{\boldsymbol{F}}) > 0$, then the nonlinear system is not locally asymptotically stable. Otherwise no conclusion can be made.

This provides for a simple criterion which just involves analysing the eigenvalues of the Jacobian of the force vector.

3.8. Defining an illumination pattern

To define a multi-colour illumination pattern we have to choose a set of modes addressed by the lasers. Since a specific mode with position frequency nk is denoted by its index n, the set of modes can be specified by an index set $I \subset \mathbb{N}$. Moreover, we have to fix the pump strengths η_n, which we summarise by a vector $\boldsymbol{\eta}$.

For instance, by choosing $I = \{1, 2, 3, 4, 5\}$ and $\boldsymbol{\eta} = \eta(1, 0, 1, 0, 1)$ the first, third and the fifth mode are pumped with the same effective pump strength η, while all other modes are not pumped. Thus in case of equal pump strengths, a certain pattern can be identified with a sequence of 0's and 1's (i.e. off/on).

Chapter 4.

Self-ordered states and light scattering of particles in a multimode field

In a first approach to understand the behaviour of atoms in a multi-mode field, we look for stable atom configurations and light fields for fixed atom positions under multi-colour pumping. We restrict ourselves to few particles and low-order cavity modes, such that we can easily visualise the stationary points and the amount of scattered light depending on the particle positions for a few instructive examples. We assume red detuning ($\delta_a < 0$) leading to high field seeking particles. For fixed atom positions it makes sense that the field has already reached its steady state (3.28). As discussed in Section 3.7, there is no collective potential yielding the force on each particle. Therefore we invoke the stability criterion for determining the stability of equilibrium points, which also implies that in the over-damped limit the atoms would dynamically find exactly those stable points.

Analytically, from (3.31), (3.27) and (3.28) we know that equilibrium points have to fulfil the equation

$$\sum_n k_n \eta_n^2 \cos(k_n x_i) \times \\ \times \left[U_0 \left(\sin(k_n x_i) \left(\sum_j \sin(k_n x_j) \right)^2 - \sum_{j,n} \sin(k_n x_j) \sin^2(k_n x_k) \right) + \delta_c \sum_j \sin(k_n x_j) \right] = 0 \tag{4.1}$$

for all i, where we assumed $\eta_n \in \mathbb{R}$. For $\delta_c < 0$ and if U_0 can be neglected, that is if $|U_0|N \ll |\delta_c|$, we obtain the simplified expression

$$F_i \propto \sum_{n,j} k_n \eta_n^2 \cos(k_n x_i) \sin(k_n x_j) = 0 \qquad \forall i. \tag{4.2}$$

For finding the stable points, in principle we have to solve this equation to obtain the equilibrium points. Next, by analysing the eigenvalues of the Jacobian of the expression above, we can decide which of the solutions are stable.

However, even with those approximations this transcendental equation is very difficult to solve analytically for more than one mode. Therefore, we will be mostly forced to retreat to numerical studies in the following.

While moving on from the simple single-colour to the multi-colour set-up, we will observe which qualitative changes occur.

4.1. Single-colour

We first check how the well-known single-colour case looks like in our very simplified model. For negligible U_0, this case can still be solved analytically for an arbitrary particle number N, as shown in Appendix B. The configuration is stable when all atoms are either at wells where $x = \lambda/4 + m\lambda$ or $x = 3\lambda/4 + m\lambda$, where $\lambda = 2\pi/k$ is the wavelength of the only involved cavity mode and $m \in \mathbb{Z}$. Due to periodicity, wells shifted by λ are totally equivalent and atoms in those wells scatter with same phase. This result is not very surprising: Each well corresponds to one of the two equivalent chequerboard patterns with opposite scattered phase, as discussed in Section 2.3.

Numerically, the stability criterion is straightforwardly implemented allowing us to find points where the forces on all particles vanish even without neglecting U_0. For two particles, these stable points can be visualised in a 2D-plane. This is done in Fig. 4.1, where we plot the stable points and the zero-force lines underlaid with the scattered light intensity $|\alpha(x_1, x_2)|^2$ within one wavelength.

The results are the same as in the analytical calculation: We obtain two equivalent stable points at $(\lambda/4, \lambda/4)$ and $(3\lambda/4, 3\lambda/4)$. Moreover, from the background plot we see that those configurations maximise the scattering. At $(\lambda/4, 3\lambda/4)$ and $(3\lambda/4, \lambda/4)$ the light scattered by the particles destructively interferes.

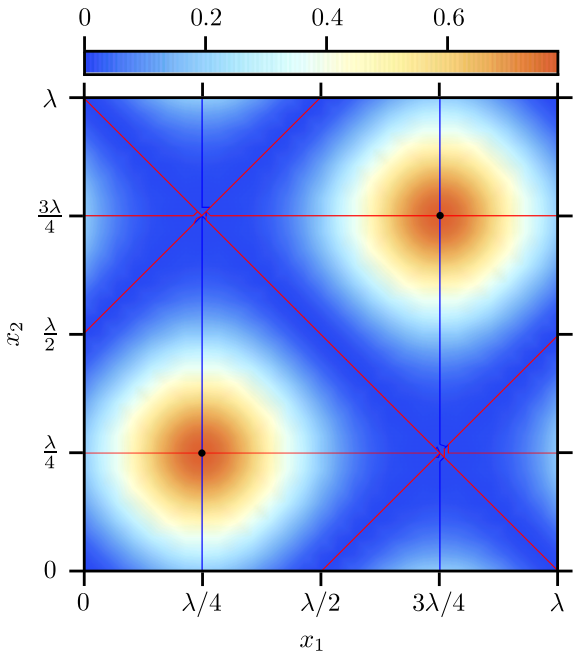

Figure 4.1.: Black dots indicate the stable configurations for two particles illuminated by a single laser as function of their positions x_1 and x_2 within one wavelength λ of the pumped mode. The density plot shows the scattered light intensity $|\alpha(x_1, x_2)|^2$ and the contours give zero-force lines for each particle. In the single frequency case there are two equivalent stable configurations at $(x_1, x_2) = (\lambda/4, \lambda/4)$ and $(3\lambda/4, 3\lambda/4)$ within one wavelength, scattering with opposite phase of each other. The parameters are $\eta = 5\kappa/8$, $NU_0 = -\kappa/10$, $\delta_c = NU_0 - \kappa$.

4.2. Multi-colour

Now we add pump lasers of different colour (i.e. frequency) and observe which qualitative changes of the scattered light pattern and the distribution of the stable points occur. For illustration in this section we use the lowest modes $n \in \{1, 2, 3, 4, 5\}$, where the modes are pumped with equal strength, which allows us to define a certain illumination pattern by a sequence of five 0's and 1's. The total scattered light is given by the sum of all mode intensities

$$P_{tot} = \sum_n |\alpha_n|^2. \tag{4.3}$$

4.2.1. From single-colour to multi-colour

As we have seen, for one pump frequency configurations where both particles sit on the anti-nodes with the same phase are stable. This leads to the periodic pattern in configuration space shown in Fig. 4.2 on the left, where we pump the fifth mode $n = 5$ (or, given as a 01-sequence, $(0, 0, 0, 0, 1)$). We see that this is only a continuation the

pattern of Fig. 4.1, where we had $n = 1$.

Now we proceed to the multi-colour case: Adding more pump lasers with the same effective pump strength close to the modes with $n = 1, 3, 4$ (resulting in the pattern $(1, 0, 1, 1, 1)$), on the one hand shifts existing stable points and, on the other hand, creates some new stable points (see Fig. 4.2 on the right). Most importantly, however, the amount of scattered light varies for different stable configurations such that they cease to be equivalent, giving rise to a complex landscape with many different local scattering maxima. This also implies that the trapping strength is different. Hence, we can already anticipate that the particles are more likely to end up in a high-scattering configuration if randomly distributed in the cavity.

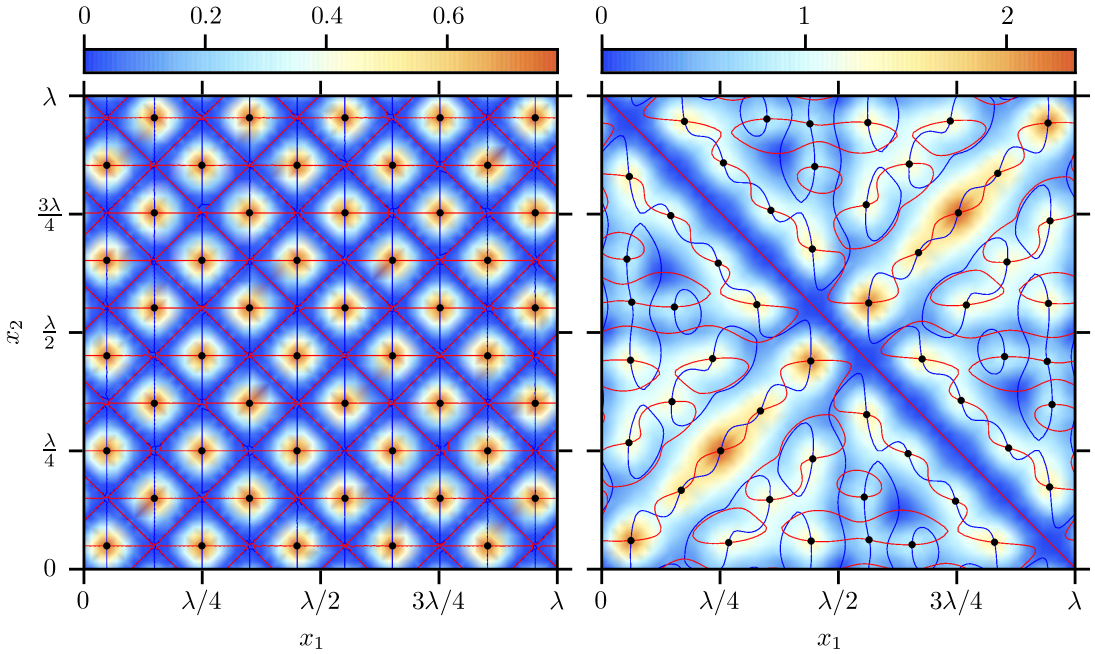

Figure 4.2.: Scattered light intensity and stable configurations (black dots) for two scatterers as function of position within one wavelength of the fundamental mode. The density plot shows the associated cavity light intensity P_{tot} and the contours give zero-force lines for each particle illuminated with frequencies near the five lowest order modes ω_n, $n \in \{1, 2, 3, 4, 5\}$. On the left we only pump at the 5-th mode, i.e. $\boldsymbol{\eta_l}/\eta = (0, 0, 0, 0, 1)$, while on the right four modes are pumped, i.e. $\boldsymbol{\eta_r}/\eta = (1, 0, 1, 1, 1)$. The parameters are as in Fig. 4.1.

4.2.2. Composition of a pattern

Obviously, the complicated irregular intensity pattern in the multi-colour set-up P_{tot} comes from adding up several single-frequency patterns with different periodicity, between which the particles have to find some compromise configuration to maximise scattering.

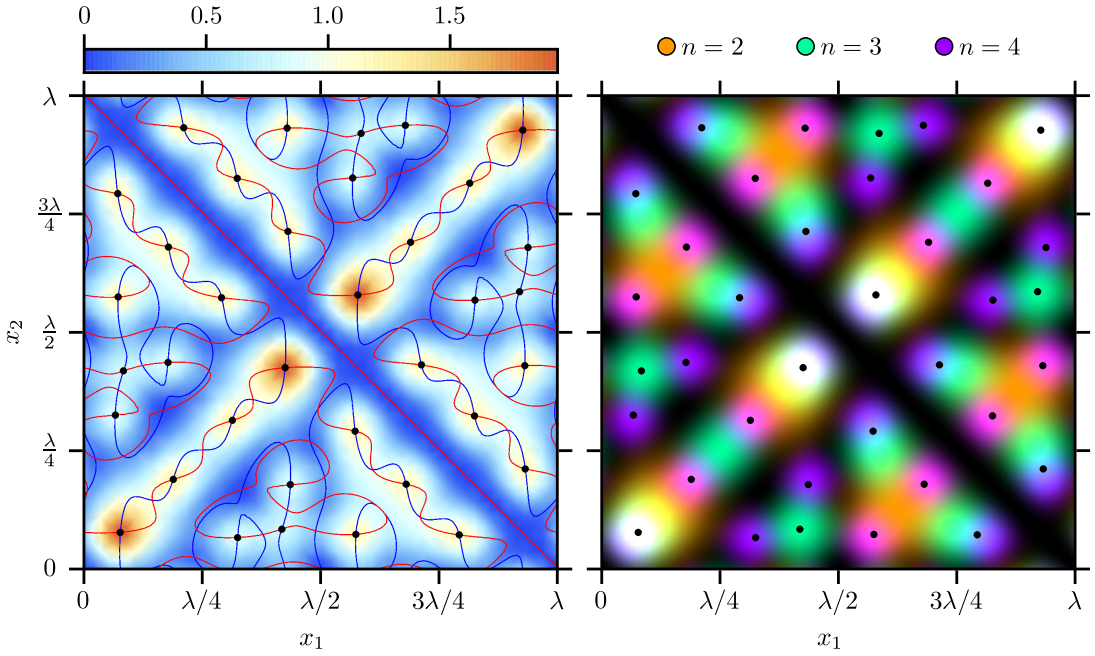

Figure 4.3.: Composition of an intensity pattern for 3 pump frequencies $\boldsymbol{\eta}/\eta = (0, 1, 1, 1, 0)$. On the left we plot the total scattered light intensity P_{tot}, stable points and the zero-force lines as in Fig. 4.2. On the right we colour-code the different mode intensities, which allows us to distinguish between the modes. In white areas all three modes oscillate, corresponding to intensity maxima in the left picture. The parameters are as in Figs. 4.1 and 4.2.

For instance, the pattern invoked by the illumination $(0, 1, 1, 1, 0)$ in Fig. 4.3 (left) is composed of the single-frequency patterns in Fig. 4.4. Clearly, the positions with optimum scattering do not necessarily coincide, which can be seen in Fig. 4.3 (right), where the three modes involved are colour-coded by three complementary colours, and mode overlapping is visualised by additive colour mixing. As we would expect, at the points of highest scattering all modes overlap, resulting in white spots in the plot.

In multi-colour patterns encountered so far we observe that the strongest scattering occurs when both particles are at the same place (i.e. $x_1 = x_2$), effectively resembling the case of one particle with stronger coupling strength. To understand this from formulas, we rewrite the mode field for two particles in relative coordinates $X = \frac{1}{2}(x_1 + x_2)$ and $\bar{x} = x_1 - x_2$, yielding

$$\alpha_n(X, \bar{x}) = \eta_n \frac{2\sin(k_n X)\cos(k_n \frac{\bar{x}}{2})}{\delta_c - 2U_0[\sin^2(k_n X)\cos^2(k_n \frac{\bar{x}}{2}) + \cos^2(k_n X)\sin^2(k_n \frac{\bar{x}}{2})] + i\kappa}. \tag{4.4}$$

Neglecting U_0, the basic form of a single-mode intensity is thus given by the square of the enumerator $|\alpha_n|^2 \propto \sin^2(nkX)\cos^2(nk\frac{\bar{x}}{2})$. With respect to $\bar{x}$, this expression is always maximal when both particles are at the same position $\bar{x} = 0$ (or, due to periodicity, some integral multiple of λ apart). As this is valid for all n, also the total scattered intensity

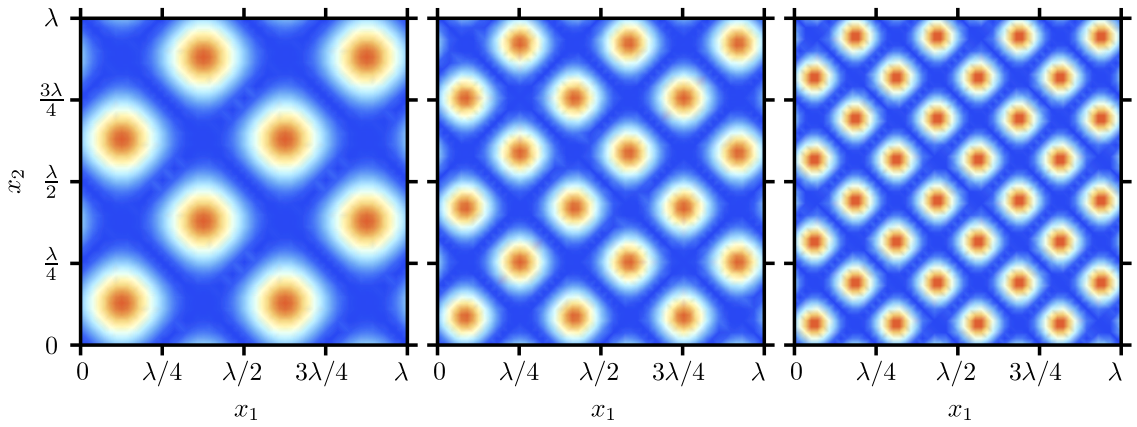

Figure 4.4.: Single mode intensities $|\alpha_2|^2$, $|\alpha_3|^2$ and $|\alpha_4|^2$ of the modes building up the multi-colour pattern generated by the illumination $(0, 1, 1, 1, 0)$ shown in Fig. 4.3.

P_{tot} is maximal when $\bar{x} = 0$, which is the reason why maximum scattering occurs on the diagonal for all illuminations.

As in the single-colour case shown in Fig. 4.1, starting from any stable configuration and shifting both atoms by $\lambda/2$ results in a stable configuration again, where light with opposite phase gets scattered. This can be best seen in relative coordinates (see Fig. 4.5): The left half plane scatters with the opposite phase of the right half plane, where stable configurations separated by $\lambda/2$ in the X-direction are equivalent counterparts.

As mentioned before, maximum scattering occurs at $\bar{x} = -\lambda, 0, \lambda$ and low scattering at $\bar{x} = \pm\lambda/2$. Obviously, the pattern is symmetric around $\bar{x}$, which corresponds to invariance with respect to particle exchange.

4.2.3. Three particles

Already in the two particle case there exist a wealth of different complex patterns, even when using equal pump strengths. Of course, with three particles those patterns get much more complicated. However, we can still graphically depict the location of the stable points by small spheres in a cube of edge length λ, as in Fig. 4.7, where the colour and size of the spheres stand for the total scattered light P_{tot}. As for two particles, most light is scattered on the diagonal ($x_1 = x_2 = x_3$).

In the right pictures of Fig. 4.2 and 4.7 the same illumination $(1, 0, 1, 1, 1)$ is governing for two and three particles, respectively, and thus allows us to compare those two cases. Obviously, the maxima on the diagonals are identically distributed, but off the diagonal there are much more possible stationary distributions of particles in the three particle case. This meets our expectation that the number of stable points strongly increases with the particle number, but we did not find a corresponding scaling law.

In realistic systems, there are usually large ensembles of particles with a huge configuration space and many stable points. We will make use of this fact in the Chapter

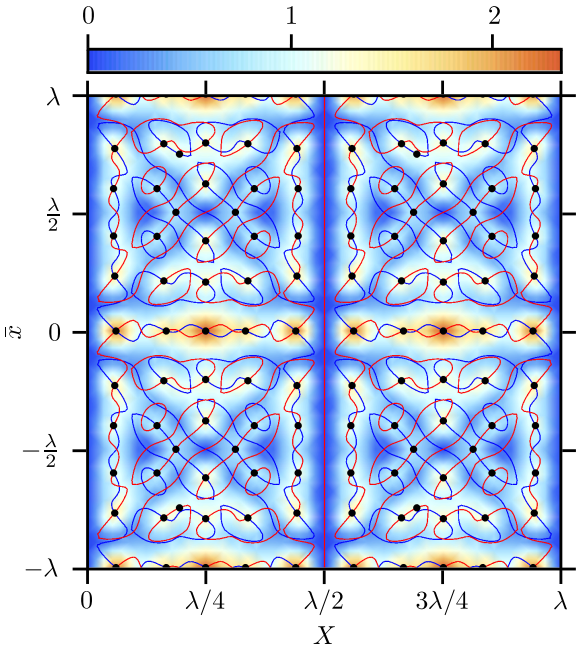

Figure 4.5.: Here the situation of Fig. 4.2 (right) is depicted in relative coordinates $X = \frac{1}{2}(x_1 + x_2)$ and $\bar{x} = x_1 - x_2$. Maximum scattering occurs for $\bar{x} = -\lambda, 0, \lambda$.

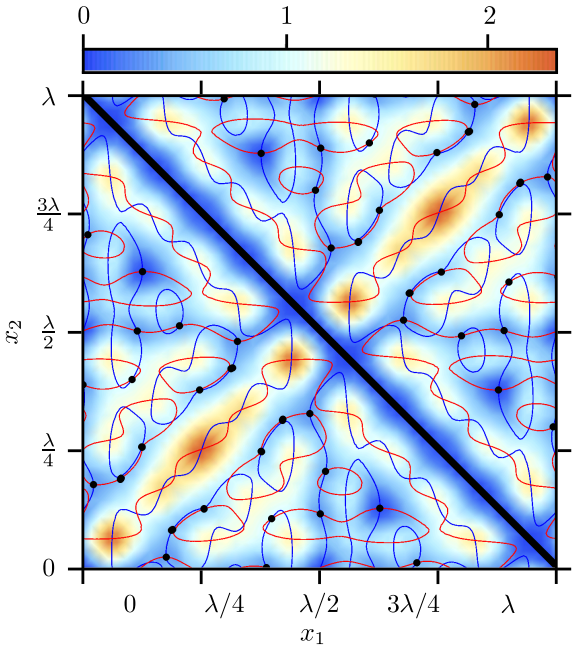

Figure 4.6.: When $\delta_c > 0$, the stable points are at scattering minima, thus also configurations on the black line are stable. We choose $\delta_c = \kappa$, while the illumination $\boldsymbol{\eta}/\eta = (1, 0, 1, 1, 1)$ and the remaining parameters are the same as in Fig. 4.2.

5.

4.2.4. Order parameter

For larger particle numbers we cannot graphically depict the stable points anymore. Hence we need qualitative measures for the grade of order of a certain configuration.

The simplest measure of order with respect to the n-th mode is the order parameter as defined in [7]

$$\Theta_n = \frac{1}{N} \sum_j \sin(k_n x_j). \tag{4.5}$$

For perfect ordering it adopts the values 1 and -1, depending on which of the two equivalent ordered configurations prevails. For a homogeneous distribution, in contrast, we have $\Theta_n = 0$ for all n. If we neglect U_0, the order parameter is proportional to the field $N\Theta_n \propto \alpha_n$.

The total order parameter

$$\Theta_{tot} = \sum_n |\Theta_n| \tag{4.6}$$

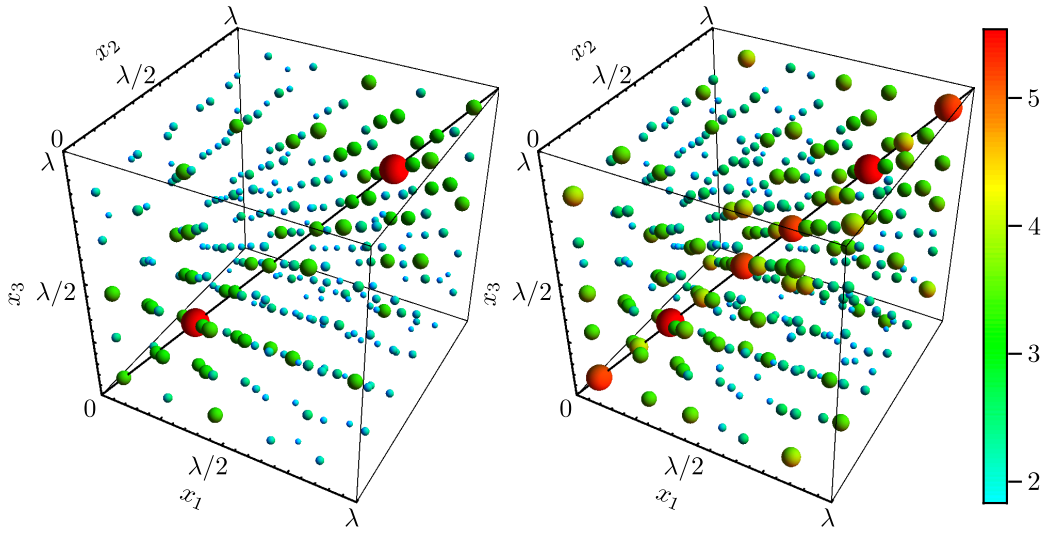

Figure 4.7.: Stable equilibrium configurations for three particles represented by spheres, whose size and color encode the amount of scattered light P_{tot} in this configuration. Illumination is set to $\boldsymbol{\eta_l}/\eta = (1, 0, 1, 0, 1)$ on the left and $\boldsymbol{\eta_r}/\eta = (1, 0, 1, 1, 1)$ on the right with the other parameters fixed as in Fig. 4.2.

measures how well the particles are adapted to all modes, i.e. how good the compromise between adaptation to each mode is. This quantity is related to P_{tot}, and for $U_0 \approx 0$ their maxima are at the same place. A homogeneous distribution leads to $\Theta_{tot} = 0$, but the maximum value is not so easy to determine and differs for various illuminations. It can get as large as the number of modes for some special illuminations (e.g. all n's odd/even), however, generally the maximum value is lower as the anti-nodes of different modes usually do not coincide. Though, it still a useful measure to compare configurations.

4.2.5. Dependence on the cavity detuning

Although we place the main emphasis in this thesis on qualitative effects and not so much the realistic implementation, it is still important to discuss the possible values and effects of crucial parameters.

Particularly the value of the cavity detuning δ_c is critical for self-organisation. We have to make sure that sign of the prefactor of the dominant λ-periodic part of the force (3.27), namely $\mathrm{sgn}(\Re\alpha_n)$, only depends on the sign of the order parameter $\mathrm{sgn}(\Theta_n)$, i.e. which of the two equivalent crystalline patterns the actual atom configuration is closer to. Since $\mathrm{sgn}(\Re\alpha_n) = \mathrm{sgn}(\Re\eta_n)\,\mathrm{sgn}(\Theta_n)\,\mathrm{sgn}(\delta_c - U_0 \sum_j \sin^2(k_n x_j))$, where $U_0 < 0$, it is sufficient to make sure that

$$\delta_c - U_0 \sum_j \sin(k_n x_j) < 0, \tag{4.7}$$

which is guaranteed when $\delta_c < NU_0$. Hence it is save to choose $\delta_c = NU_0 - \kappa$ or

$\delta_c = NU_0/2 - 2\kappa$, which are the values we used for our calculations. This topic was discussed in more detail in [7].

The denominator of $|\alpha_n|^2$

$$\left(\delta_c - U_0 \sum_j \sin^2(k_n x_j)\right)^2 + \kappa^2 \tag{4.8}$$

shows that scattering is resonantly enhanced when δ_c is suitably shifted from the bare cavity resonance $\delta_c = 0$. Scattering at perfect ordering ($\theta = \pm 1$) is maximal when $\delta_c = NU_0$. However, this value is not allowed due to the above restriction, such that realistically scattering is most efficient when δ_c is slightly smaller than NU_0. With $\delta_c = NU_0 - \kappa$ we get the dependence $|\alpha_n|^2 \propto \kappa^{-2}$.

For $\delta_c \geq 0$ (and $U_0 < 0$), we also get a fixed sign of $\delta_c - U_0 \sum_j \sin^2(k_n x_j)$ which would allow self-organisation at least under the aspects considered before. In this case the stable configurations result in minimum scattering, which can be seen in Fig. 4.6.

Chapter 5.

Adaptive dynamics

In the previous chapter we studied light fields and forces at fixed particle positions, where points of vanishing force give equilibrium positions. The equations of motion (3.26), however, also describe dynamical properties of the system. In this chapter we will numerically examine the dynamical adaptation of the particles to static illuminations under the influence of noise and to time-varying illuminations. Since stable configurations are associated with high scattering, we expect that adaptation gradually increases the amount of scattered light and thus optimises light collection.

As known from the single mode case the delayed field response during the self-ordering for negative cavity detuning induces friction (i.e. cavity cooling) such that the system reaches a steady state [8]. Although finding suitable parameter ranges where system inherent cooling works efficiently in the multi-colour case is an interesting task as such, in this work we are qualitatively interested in the adaptation of the particles to different illuminations. Thus we simply mimic cavity cooling as well as other possible damping effects e.g. by a background gas or optical molasses in the system by adding an effective linear friction force as in (3.29), such that we can easily control the friction strength by a parameter μ. This is only an approximation to the actual full dynamics, but will guide the system towards a stable or at least metastable state.

5.1. Static illumination with noise forces on particles

In any real system damping is accompanied by noise forces on the particles. For a static multi-frequency illumination pattern, we expect that this renders the stationary configurations metastable and that the particles will eventually leave any such configuration and evolve towards another metastable state, which possibly results in stronger trapping and scattering. As for $\delta_c < 0$ there is a tendency towards high scattering configurations, on the long haul this process should lead to a dynamical optimisation of scattering for the applied illumination, that is the particles should be able to find the global scattering maximum after venturing through other parts of configuration space.

In our model, noise is natively included in the full dynamics (3.25) via the Wiener

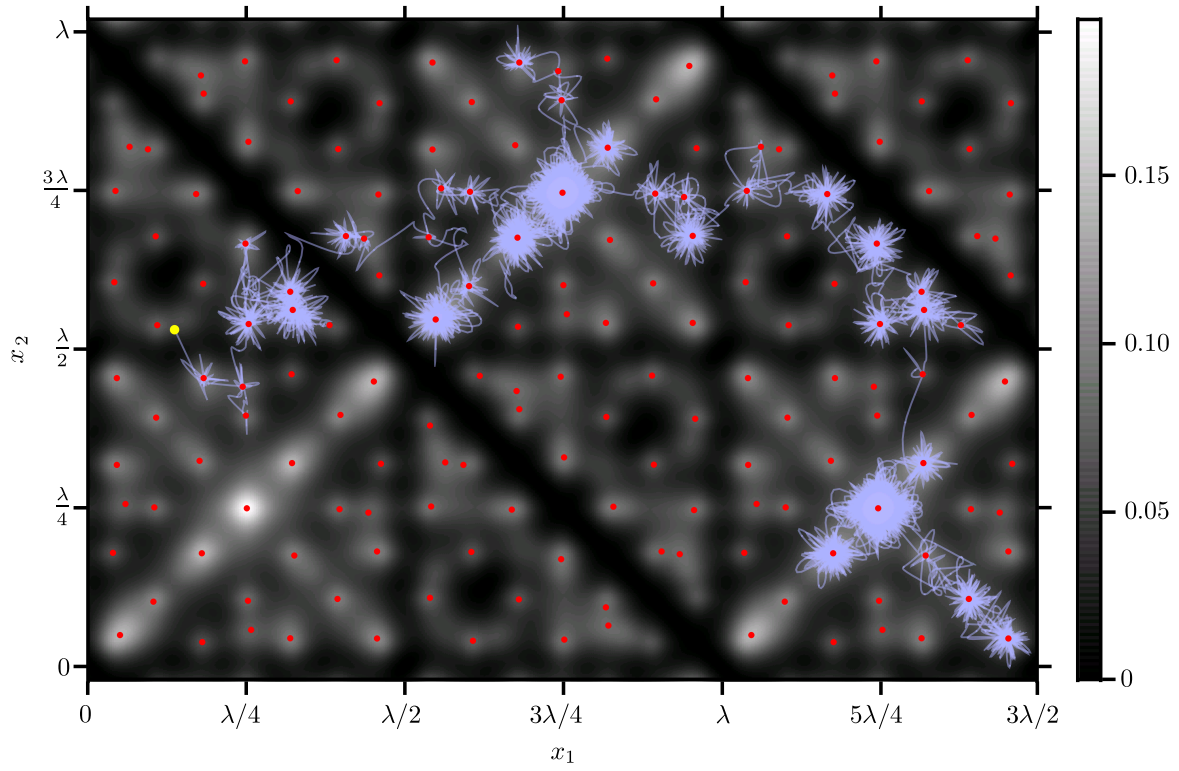

Figure 5.1.: Typical trajectory of two particles in static illumination $\boldsymbol{\eta}/\eta = (1, 0, 1, 1, 1, 0, 1)$ experiencing random momentum kicks at time intervals $\Delta t = 2/\kappa$ and friction $\mu = 2\kappa$, where the yellow dot indicates the initial position. As in Fig. 4.2 the background density shows the scattered intensity P_{tot} and red dots indicate stable equilibrium positions in the strongly damped limit. The other parameters are $\eta = \kappa/5$, $NU_0 = -\kappa$ and $\delta_c = NU_0/2 - 2\kappa$.

processes $\mathrm{d}W_{1,n}$ and $\mathrm{d}W_{2,n}$ representing field fluctuations as derived in [8], which can be traced back to the damping of the field mode via cavity losses. While in a quantitatively correct description these and even more noise sources would have to be carefully modelled and scaled, here we simply introduce noise forces as random momentum kicks on individual particles, as used for Brownian motion. In our simulations the particles evolve according to the equations of motion with the additional friction term proportional to μ, but after a fixed time step Δt they experience a momentum kick whose strength and direction are randomly chosen from a normal distribution with a width proportional to $\sqrt{\Delta t}$ and an associated temperature. This simplified model still leads to the qualitative effect discussed above.

In Fig. 5.1 we show a typical simulated trajectory for two scatterers over an extended time. While the particles rapidly evolve in the dark areas, the trajectory concentrates around bright areas of the background picture P_{tot}, denoting local scattering maxima. The system thus explores a large volume of configuration space but preferentially stays at points of strong scattering. That is because it takes more time to diffuse out of strongly

scattering trapping wells as compared to others. Note that the background picture including the red dots indicating stable points is obtained by using the techniques from the previous chapter, that is assuming over-damped motion in the bad cavity limit. For a dynamic field, which we simulate now, scattering does not solely depend on the particle configuration and thus one cannot make a simple picture like that. Especially, from the trajectory we see that there are no stable points where the particles stop. Nevertheless, for relatively large μ, actual scattering along the trajectory at least qualitatively corresponds quite well to the background picture and particles at least tend to stay close to red dots, which justifies the inclusion into the figure for illustrative purposes.

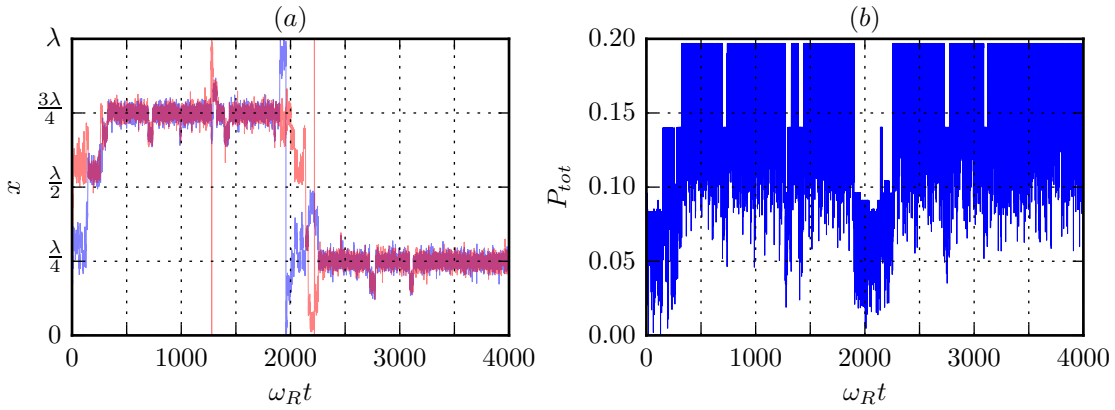

Figure 5.2.: Time evolution of (a) the positions of the two particles modulo λ and (b) the scattered light intensity P_{tot} for the trajectory of Fig. 5.1 with $\omega_R = \kappa\pi^2/10$. The particles spend most time at points of high scattering at $x_{1,2} \approx \lambda/4$ or $3\lambda/4$.

The effect of localisation near scattering maxima is displayed more quantitatively in Fig. 5.2. In picture (a) we plot the time evolution of the two atom positions modulo λ (due to periodicity). Most of the time both particles are at the same position, hopping between $\lambda/4$ and $3\lambda/4$, which correspond to the positions with highest scattering. This becomes apparent from picture (b), where we observe that the total scattered light P_{tot} drops when the particles leave these positions.

Due to this behaviour the system can be considered an adaptive light collection system: Given any multi-frequency illumination, the particles dynamically adapt such that light scattering into the cavity (and thus the cavity output field) is maximised for most of the time.

5.2. Varying pump light

In this section we consider time-varying multi-colour pump light. For simplicity, we regard over-damped dynamics without noise and the field in the bad cavity limit. More

specifically, we choose a set of illumination patterns and consecutively apply them to our system, each one long enough such that the system relaxes to a steady state before switching to the next illumination. Pumped with the first illumination, the particles will soon find a stable point close to their initial configuration, which locally maximises scattering. When we change the illumination conditions and apply a new pattern, the current particle configuration is most probably not stable anymore, which forces the particles to a new stable point with respect to the new illumination. Repeating this process in a periodic or random sequence, we investigate the time evolution of scattered light and atom configurations. The tendency should be the same as in the previous section: Scattering is expected to increase since strongly scattering wells have larger depths and basins of attraction. However, now the particle have to adapt to several multi-colour patterns. Under this viewpoint, we want to find out if and under which conditions the particles evolve towards configurations which result in significantly larger scattering than in the beginning.

5.2.1. Periodic pump sequences for three particles

In a first simple and instructive example we consider three particles, which are consecutively illuminated by five illuminations containing only the seven lowest order modes $n \in \{1, 2, 3, 4, 5, 6, 7\}$ in a fixed, periodic sequence. In this case we can think of changing an illumination as subsequently imposing five different optical potential landscapes as in Fig. 4.7: Under a certain illumination particles relax to a close-by sphere, then the distribution of spheres changes (i.e. illumination is changed) and the particles find a new sphere. This process continues in a periodic manner.

We visualise the atomic motion in a three dimensional cube in Fig. 5.3. After a few initial position changes, the atoms find a suitable closed loop in configuration space and periodically follow the illumination sequence. Due to the complexity of the optical potential landscape, for different initial positions a multitude of such loops is attained for the same illumination sequence. Particles with close-by initial configurations often enter the same loop (e.g. (c) and (d)). Also, we can see that once all particles meet, i.e. find the diagonal in Fig. 5.3 like (e) and (f), they stick together, effectively forming one particle with higher coupling strength. In all example loops at least two particles meet, which is due to the (unrealistically) low particle number leading to a small configuration space, and the use of low-order modes leading to relatively few stable points. However, as we have seen in Fig. 4.7, scattering is high for such configurations. Note that the deterministic behaviour demonstrated in this example is due to simplifications we made. In realistic systems, noise would eventually cause the particles to separate and leave a closed loop.

Each loop has a characteristic output intensity for each mode $|\alpha_n|^2$, which could be used as signatures to experimentally distinguish between them. For the example loops in Fig. 5.3, these intensity sequences are shown in Fig. 5.4. Obviously, (c) and (d) are equivalent after the first switch, which is already clear from the trajectory as they end

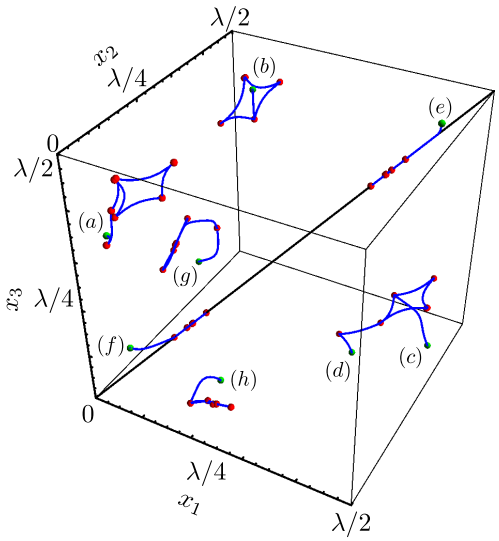

Figure 5.3.: Configuration space trajectories for three particles with periodically time-varying illumination starting at different initial positions denoted by green dots and the letters (a)-(h). $\boldsymbol{\eta}/\eta$ periodically cycles through five different illumination conditions given by $(1,0,1,0,0,0,1)$, $(0,1,1,0,1,1,0)$, $(0,0,1,0,1,0,0)$, $(0,1,1,1,1,1,0)$, $(1,1,1,1,0,1,0)$. The illumination changes after the system has reached a stable point (red dots). The parameters are $\eta = \kappa/5$, $NU_0 = -\kappa$ and $\delta_c = NU_0/2 - 2\kappa$.

up in the same loop. However, due to symmetry also (a) and (b) have the same form as (c) and (d) at least after the second switch. Also the two loops on the diagonal (e) and (f) are equivalent.

Of course, due to its periodic nature the intensity does not increase during the process as the same loop is repeated many times. This changes if some randomness is introduced to the dynamics. Such fluctuations can originate from noise as in the previous section or from a randomly varying pump light as follows.

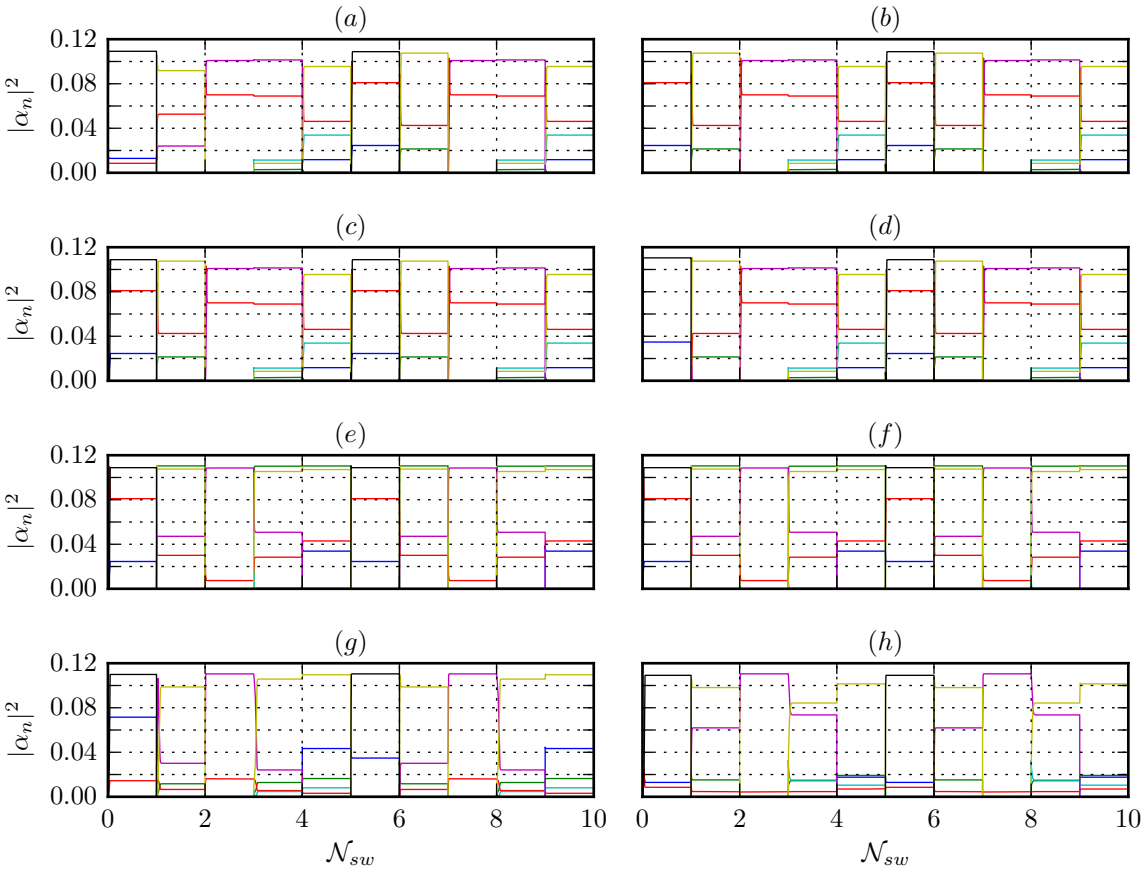

Figure 5.4.: Output intensities for each mode of the loops with initial conditions (a)-(h) as shown in Fig. 5.3 for 10 switches of the illumination $\mathcal{N}_{sw}$. (a), (b), (c) and (d) are equivalent to each other after the first switch. Also (e) and (f) are the same due to symmetry.

5.3. Time evolution of larger ensembles with varying pump light

All the previous examples dealt with low particle numbers interacting with few low order cavity modes, which illustrate the basic physical mechanism of multicolour self-ordering. More interesting and realistic examples appear for large particle numbers with a correspondingly high-dimensional configuration space, and many high-order modes causing a huge number of stationary states. In such a scenario it is very unlikely for the particles to find a global scattering optimum, and many intermediate configurations appear. As we are dealing with classical particles, the necessary computing resources stay reasonably small even for 1000 particles.

Again, for one realisation we use five illumination patterns where the pumped mode

frequencies nk are chosen such that $n \in I = \{n_1, n_1 + \Delta n, ..., n_1 + 99\Delta n\}$ with $n_1 = 1003$ and $\Delta n = 7$, which only involves high-order modes. When choosing I we tried to avoid that the used frequencies are multiples of each other by using odd numbers for n_1 and Δn. As all modes are pumped with equal strength, we can define an illumination by a sequence of 1's and 0's of length 100. Practically, for one set of illuminations we produce five random 01-sequences with equal probability of 1 and 0, such that in one illumination approximately 50 frequencies are actually pumped. For simplicity we will use the index n' to denote the modes, where $n' = 1$ corresponds to $n = n_1$, $n' = 2$ to $n = n_1 + \Delta n$ and so on.

In the following discussion we will usually use 100 particles ($N = 100$), which are initially randomly distributed in an area of length of the fundamental wavelength $\lambda = 2\pi/k$. Although more particles would give statistically more reliable results, also computing time increases, which made us settle at 100 particles as a compromise.

5.3.1. Optimum of one illumination

To find out which orders of magnitude we should expect from the scattered intensity, we calculate some rough estimates.

By pumping a single mode to which the particles are perfectly ordered we get a maximum scattered intensity of

$$P_0 = |\alpha_{max}|^2 = |\eta|^2 \frac{N^2}{|\delta_c - NU_0 + i\kappa|^2}, \tag{5.1}$$

which does not depend on n as we use equal pump strengths.

If there was a position where the light is scattered maximally into all modes the photon number in the cavity would be

$$P_{opt} = \sum_n |\alpha_{n,max}|^2 = \sum_n |\eta_n|^2 \frac{N^2}{|\delta_c - NU_0 + i\kappa|^2}, \tag{5.2}$$

which for equal pump strength is simplified to

$$P_{opt} = N_m |\eta|^2 \frac{N^2}{|\delta_c - NU_0 + i\kappa|^2}, \tag{5.3}$$

where N_m is the number of pumped modes ($N_m \approx 50$). Practically such a configuration does not exist, as there is usually no point where all modes have an anti-node.

For the parameters used so far in this chapter ($\eta = \kappa/5$, $NU_0 = -\kappa$ and $\delta_c = NU_0/2 - 2\kappa$), $N = 100$ and $N_m \approx 50$ we obtain

$$P_0 \approx 120 \qquad P_{opt} \approx 6000,$$

where P_{opt} can vary for about ± 1000 if we assume that the number of pumped modes varies for about 10.

We expect that the actual scattered intensity is well below P_{opt} but higher than P_0.

5.3.2. Illumination sets

As mentioned before, we will use the following illumination sets with position frequencies nk, where $n \in I = \{n_1, n_1 + \Delta n, ..., n_1 + 99\Delta n\}$ with $n_1 = 1003$ and $\Delta n = 7$, and I contains 100 elements. One specific illumination $\boldsymbol{\eta}/\eta$ is given by one line, i.e. a sequence of length 100, which specifies if a certain frequency in I is switched on or off. The yellow highlighting marks pump frequencies which are switched on in all illuminations of a set. Later we will see, that the value of those frequencies has a crucial impact on the adaptive behaviour of the particles.

Illumination set (1):

```
1  0000100100101110011010101011101 0 0011100010101010000001111011101001000011010011 1 1 1 101000000100111001
2  0100111110011111100110010010011 0 1000111101100010001111001111100000011000011001 1 0 1 110111100110110100
3  1100001110001010011011011110000 0 0111001000001011100100111011011010101011110000 1 1 1 011010100110011100
4  1101000001101100101100010000011 0 0001000011011100110100101000101000100000011111 1 1 1 111000110101010001
5  0001110111100110101011001111010 0 1100101100001010101010000110010111010100001001 1 0 1 010101100000000110
```

Illumination set (2):

```
1  1101000000001010001111101111010 1 1 0 1 0100 1 0 1 1101000101100010100111000110100110010011100001000101101011
2  1001000001001111001100010101001 0 1 1 1 0100 1 0 1 0100111111100101100110010101000101110011111100001110010111
3  0011100001011000110111111000010 0 1 1 1 0011 1 0 1 0000101011001010010000001010100000011010101010010000111000010
4  1010100111101000001001010101001 1 1 0 1 0100 1 0 1 1110011000100101100111000101111010000100100101111111011101
5  1110000111000001110101001011100 1 1 0 1 0011 1 1 1 0110110000111010001001110001010111010010101110011010100010
```

Illumination set (3):

```
1  10 1 1011001101011101 0 1101 1 1010010011110010100010100011111010111010000000100100111100100110001101110 1
2  11 1 0010000000111110 0 1101 1 1110010101010011100001010000011100000000001111101000001000101011011011011 1
3  11 1 0011110101100110 0 1110 1 1000001100111100110110001001010110111001100100010100000100010010110011001 0
4  00 1 0101101100011010 0 0011 1 1110111001100001111110000110110011011100001000101001000011000001111010101 0
5  01 1 0101100001001001 0 1110 1 0000000001100100000010000110101011011111001110001001110111001110100000111 1
```

5.3.3. Periodic sequences

Connecting to the previous chapter we start with applying a periodic pump sequence of illumination set (2). In Fig. 5.5 we show the time evolution of the total scattered intensity P_{tot} and the order parameters Θ_n for one random initial atom distribution. Of course, due to the more complicated mode landscape it takes more illumination switches than for the low particle and mode-order case in the previous section until a stable loop is found. For this specific initial particle distribution we find that after 15 switches the time evolution gets periodic. Taking a look at the order parameters reveals that for each illumination one specific order parameter dominates: particles order according to mode $n' = 99$ (blue) for illuminations 1-3 and to mode $n' = 91$ (black) for illuminations 4-5. Hence it is also not surprising that the total scattering intensity at stable points ranging from 145.2 to 157.2 is only a little higher than that of a single laser with perfect particle order $P_0 \approx 120$. Also, scattering does not significantly increase from the initial value.

Let us also take a look at the form the time evolution of P_{tot}: When the illumination is changed, the amount of scattered light drops immediately to values as low as 20, as at this time the atom ordering is not suitable anymore. Then the particles find a new order corresponding to the new illumination reestablishing a scattering strength close to before. To ensure that particles reach the steady state before the next illumination change, this reordering happens very fast compared to the time between the switches, rendering the dip very narrow in the plot.

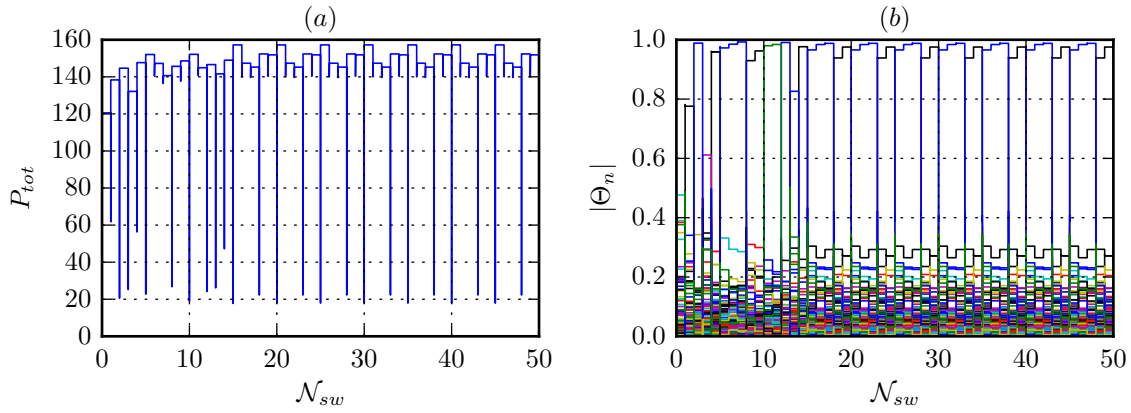

Figure 5.5.: Scattered intensity P_{tot} and the order parameters Θ_n for a fixed, periodic sequence of illumination set (2). After 15 switches the time evolution is periodic, where the period is 5 switches $\Delta\mathcal{N}_{sw} = 5$ as we apply 5 different illuminations. The parameters are as in Fig. 5.3.

5.3.4. Random sequences

When we apply random sequences of illumination of a certain illumination set, particles will not attain closed loops and the system will evolve non-predictably on a longer timescale. Due to the randomness a larger portion of configuration space is explored and we expect an enhancement of scattering, similar to the case in Section 5.1, where the randomness came from the noise forces acting on the particles.

However, an adaptation such that scattering increases significantly does only work well when certain requirements are fulfilled. In the next section we show a negative example.

One mode wins

Fig. 5.6 shows order parameters and scattered intensity for two realisations (i.e. different random sequences and initial distribution) using illumination set (1). In both cases, the particles organise mainly with respect to one mode leading to one order parameter close

to 1, while P_{tot} (ranging from 145 to 170) does not significantly increase over the single mode scattering of 120 and stagnates in the long term.

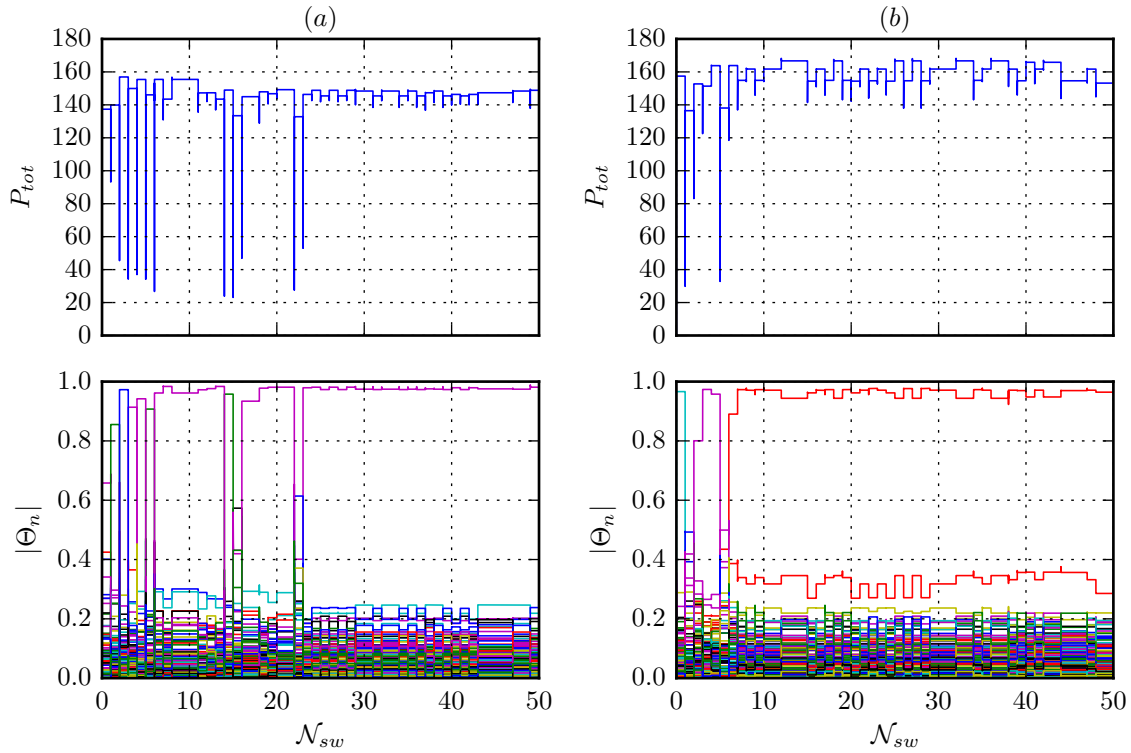

Figure 5.6.: Scattered intensity P_{tot} and the order parameters Θ_n of 100 particles which are pumped with illuminations randomly chosen out of illumination set (1) for two different realisations (a) and (b). After a few switches, the particles order according to mode (a) $n' = 82$ and (b) $n' = 80$, respectively. The parameters are as in Fig. 5.3.

In realisation (a) and (b) the dominant order parameters are Θ_{82} and Θ_{80}, respectively. Interestingly, in our chosen illumination set (1), these are exactly the highest modes which are switched on in all five illuminations marked in yellow in Section 5.3.2. Thus it becomes clear that once the particles order according to one of those frequencies, the configuration is close to a stable point under all illuminations and the particles are not forced to move significantly. However, it also hinders the particles to find a configuration which adapts to all modes and thus the scattered intensity stagnates at a low value.

Adaptation to many frequencies

To avoid such situations we find that it is sufficient to make sure that high-order modes are not switched on in all illuminations, while this is still acceptable for low-order modes. This can be explained as follows: Thinking of the mode landscape as a potential which

is the inverse of a superposition of all mode intensities, high frequencies (short length scale) tend to determine the position of the stable points while low frequencies (long length scale) only weight those, i.e. attach a depth and basin of attraction to them. In a complex system (many modes and particles) as the present, particles can quite soon adapt to a high-order mode, but only very slowly approach a configuration adapted to a low-order mode due to the huge number of stationary points in between. A high-order frequency present in all illuminations acts like a barrier on this way, stopping further adaptation as we have seen before. Also if such a barrier does not exist, particles do not eventually order according to a single low-order mode, but adaptation stops at a compromise configuration where scattering into many modes is high.

Here we present some working examples, where the scattered intensity increases significantly. We observe that this adaptation stops after some time, showing that the particles have found some dynamically stable area in configuration space.

For that we apply random sequences of the illumination sets (2) and (3), where the highest modes pumped in all illuminations are $n' = 42$ and $n' = 26$, respectively, both much lower than in illumination set (1). The time evolution of P_{tot} for one realisation is plotted in Fig. 5.7, where we observe that P_{tot} (starting from a value of about 140) is roughly monotonically increasing, demonstrating that the particles continuously improve their adaptation to the all five illuminations simultaneously. After approximately 8000 switches, this adaptation process stops and P_{tot} stays within a range of 461 to 507 with the mean value 485, which is nearly 3.5 times the initial value. The atoms stop moving significantly (see Fig. 5.7 (c)) since they have found an area in configuration space which is well adapted to all modes. This can be seen from the order parameters in (d), where after 8000 switches many reach values up to 22, which is about half of the theoretical maximum 50.

Both, the number of switches needed to reach such a state and the resulting light intensity strongly vary for different realisations. This becomes clear from Fig. 5.8 (a), where we compare three different realisations (including the one from Fig. 5.7). The green intensity stagnates after 15500 switches at a mean value of about 663, over 4.5 times larger than the initial intensity, while the blue intensity does not stagnate within integration time, but increases similarly fast as the other examples. Note that the final intensity is about one order of magnitude lower than P_{opt}.

From Fig. 5.8 (b) we observe that the number of particles in clusters $N_0 + 1$ (i.e. particles which stick together with zero distance) is to a certain extend proportional to P_{tot}. Or, put differently, the system can better adapt to many modes if the effective particle number $N - N_0$ is lower (and the resulting effective configuration space lower dimensional), which results in stronger scattering. This is consistent with the two- and three-particle case in Chapter 4, where we observed that strongest scattering occurs on the diagonals. As mentioned before, in realistic systems such clusters would be eventually split up by noise forces. Also in 2D or 3D models, such clusters can be expected to form much slower due to the larger configuration space.

This adaptive ordering can be interpreted as acquisition of memory of past illuminations.

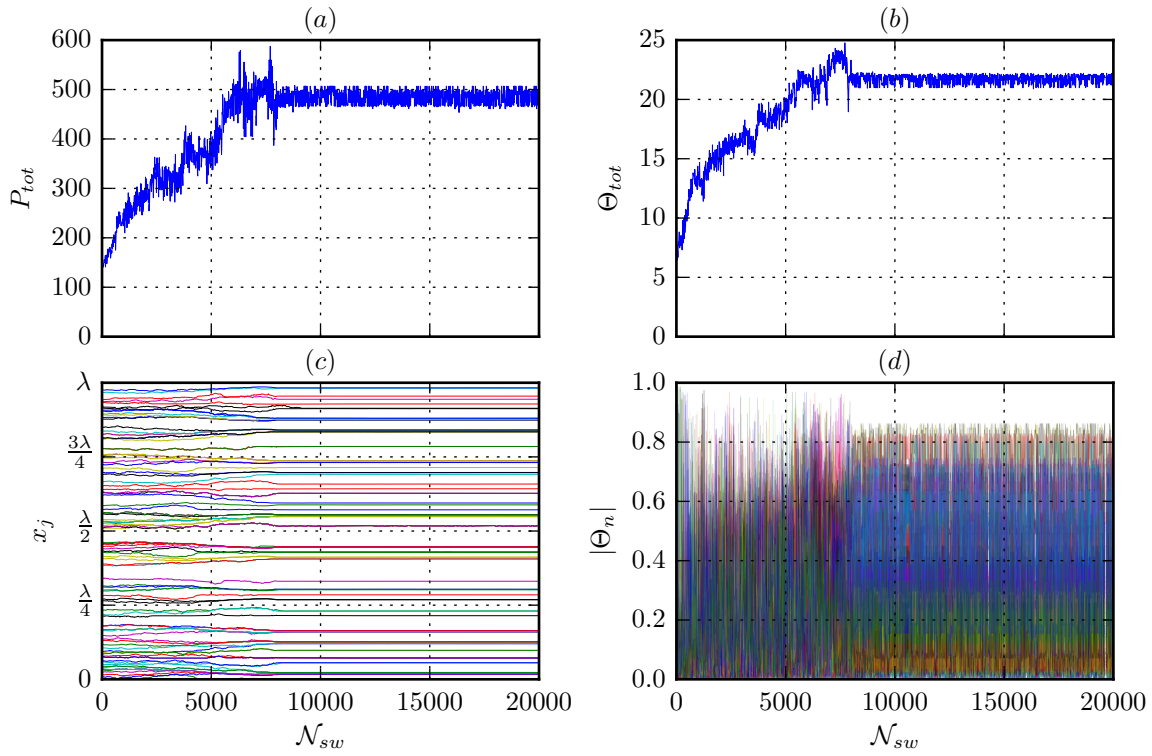

Figure 5.7.: Time evolution of (a) scattered intensity, (b) total order parameter, (c) particle positions and (d) order parameters of 100 particles pumped by random sequences of illumination set (3). After a significant increase P_{tot} stagnates, only fluctuating around a mean value of 485. The parameters are as in Fig. 5.3.

When we apply any of the five illumination patterns after a long time evolution, more light will be scattered for each configuration than for the random particle distribution in the beginning. Hence, the system remembers that this illumination has been repeatedly applied before, whereby the information is stored in the order of the atoms.

Large set of illuminations

When we apply random sequences of illuminations chosen out of a large illumination set (1000 instead of 5), the scattered intensity initially increases in a similar manner up to a value of about 500 (see Fig. 5.9 (a)). However, as each illumination is applied much less frequent (on the average 20 times instead of 4000 times for 20000 switches), a dynamically stable situation is not found within the integrated time.

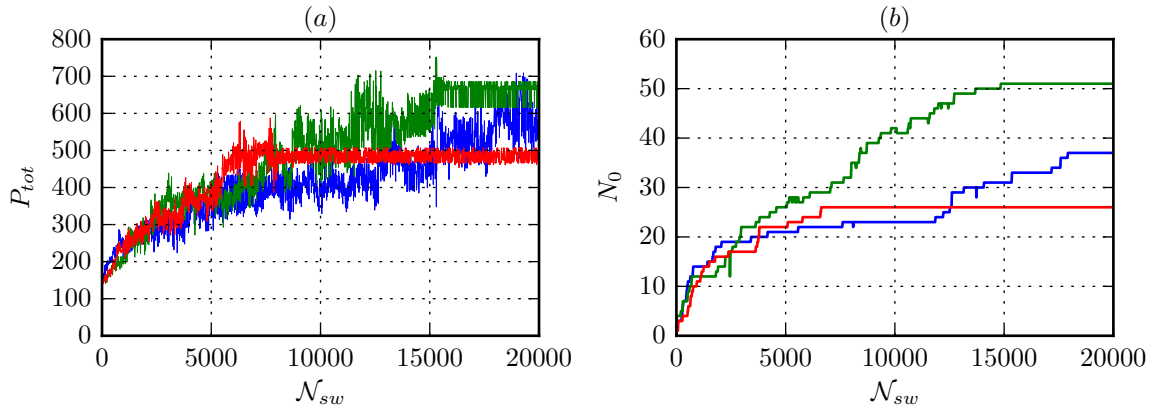

Figure 5.8.: Comparison of the time evolution of (a) the scattered intensity P_{tot} and (b) the number of particles in clusters N_0 for three realisations as in Fig. 5.7. Illumination pattern (3) was applied for the red and blue curves, while for the green curve illumination pattern (2) was used. The final value of P_{tot} as well as time after which it stagnates varies.

Pumping with more frequencies

Again, we apply random sequences of five illuminations, this time using 1000 frequencies close to nk with $n \in \{n_1, n_1 + \Delta n, ..., n_1 + 999\Delta n\}$ and $n_1 = 1003$ and $\Delta n = 7$. As before, we randomly choose five 01-sequences of length 1000 with equal probability of 0 and 1, resulting in about 500 pumped frequencies per illumination.

In Fig. 5.9 (b) we plot P_{tot} for two realisations. While the input intensity is 10 times higher than previously, the scattered intensity after 10000 switches is only approximately 2 times higher. Overall we observe an increase from about 420 to 1085, corresponding to a relative increase of only 2.5, which shows that using these illuminations is less efficient.

Using more particles

From (5.1) we see that the scattered intensity depends quadratically on the particle number, that is $P_{tot} \propto N^2$. Here we will simulate the time evolution for 1000 particles, which should result in scattering enhancement of a factor 100. In Fig. 5.10 we compare P_{tot} and total order parameters for 1000 particles under random sequences of illumination set (3) with two 100-particle simulations shown in Fig. 5.8 which are scaled accordingly and where the same illumination set has been used. However, we observe that there is no significant difference after the first 2000 switches.

Since the illumination defining the characteristic length scale of the potential landscape is the same as in the 100-particle case, more particles end up in the same well leading to stronger clustering. In this realisation, the effective particle number after 2000 switches has decreased to 201, which already gets close to $N = 100$.

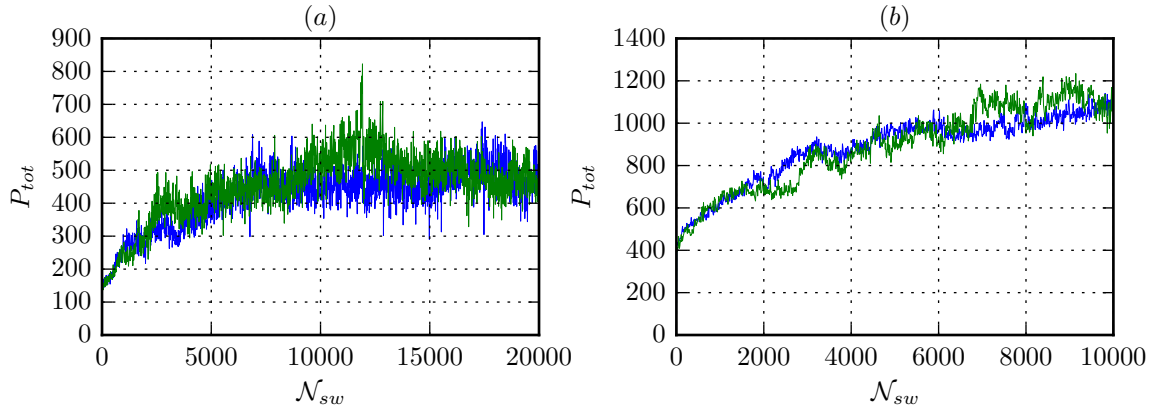

Figure 5.9.: Scattered intensity for two realisations using a random sequence of (a) 1000 illuminations with approximately 50 pumped frequencies and (b) 5 illuminations with 500 frequencies. The parameters are as in Fig. 5.3.

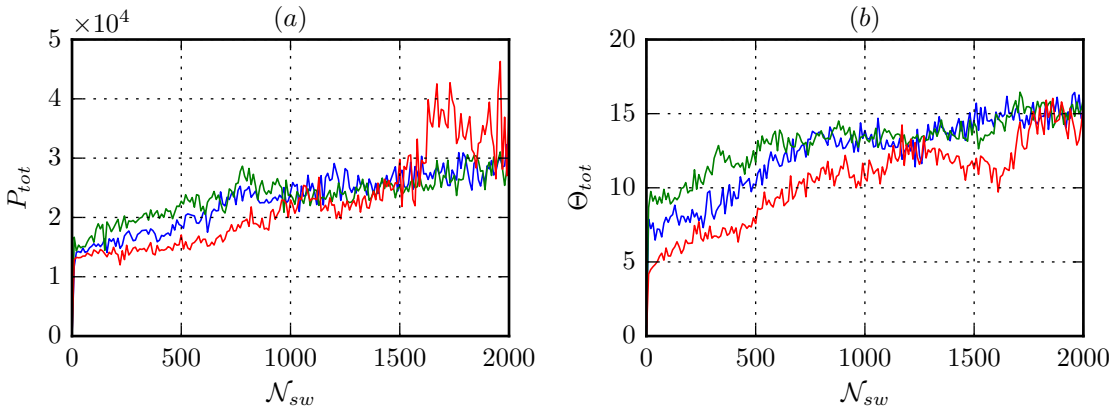

Figure 5.10.: Comparison of the time evolution of (a) the scattered intensity P_{tot} with $N = 1000$ particles (red curve) and $N = 100$ particles (green and blue curves), where the $N = 100$ curves are multiplied by 100 (that is, scaled according to $P_{tot} \propto N^2$). In (b) the total order parameters for those realisations are shown. There is no significant difference between $N = 1000$ and $N = 100$. In all three realisations illumination pattern (3) was used, while the remaining parameters are as in Fig. 5.3.

Chapter 6.

Conclusion and outlook

Polarisable particles in a high-finesse cavity which is driven from the side by a red detuned laser with a sufficiently high pump strength organise into one of two equivalent regular patterns which scatter with opposite phase. By that the system's energy is minimised while scattering into the cavity is maximised. In this work we extended the single laser drive with one frequency to a multi-colour drive where each laser scatters into a distinct cavity mode. This results in a complicated potential landscape giving rise to a multitude of stable patterns with varying scattering efficiency and stability, which leads to a wealth of intriguing phenomena beyond simple self-ordering.

Employing a simple classical model, we showed that by including momentum diffusion the particles can hop between various stable patterns, whereby they tend to stay longer in high-scattering configurations. This gradually leads towards an optimisation of scattering. When we sequentially apply several multi-frequency illuminations, the system continuously improves adaptation to find a compromise between the applied illuminations even without noise. We found that this adaptation leads to a significant increase of scattered intensity compared to a nearly homogeneous distribution. After the particles have evolved for some time, the system can react faster on a reappearing illumination pattern having memorised past conditions. Hence we can consider the system an adaptive and self-learning light collection system with built-in memory.

Experimentally, this model could be implemented in the framework of cold gases of atoms in high-Q cavities, which was also the main viewpoint in this thesis. However, one can also think of alternative set-ups using mobile nano-particles in solutions. Note that the technology needed to create many equidistant frequencies matching those of the cavity is available by using frequency combs. The emitted cavity field is an accessible quantity for experiments, allowing for real-time monitoring of the prevailing particle configuration [32, 33].

In this work we tried to qualitatively convey basic phenomenons of multi-frequency self-ordering and thus made many grave simplifications. An extension of this work could aim for a more realistic treatment of the same aspects. Particularly, it would be interesting to use system inherent cavity cooling instead of the artificially added friction

term, which together with noise would lead to a gas in a dynamical equilibrium with some corresponding temperature.

But also within these simplifications this work should be put on a more stable footing by using a more systematic approach. For instance, to make more meaningful conclusions we have to use statistical methods more extensively (e.g. averaging over a large number of realisations). Also, considering longer time evolutions would be interesting, e.g. when comparing the behaviour for different particle numbers or to see if the adaptation of seemingly non-stagnating realisations stagnates later on. Moreover, we would like to compare the actually reached value of the scattered intensity with the global scattering maximum, which we were not able to find for the general multi-particle and multi-mode case. Here one could employ numerical optimisation methods like Metropolis algorithms or try to analytically show the unproven expectation that the global maximum has to be on the diagonal of configuration space.

Finally, one could push further into the field of neural networks and explore the analogies to Hopfield networks [34], which provide a model for understanding human memory and can be used for pattern recognition.

Appendix A.

Operator correspondences for functions of the position operator

We want to rewrite a master equation containing functions of the position operator into a partial differential equation for the Wigner function $W(x,p)$. Using the operator correspondences given by (3.15), an arbitrary infinitely often differentiable function $g(x)$ of the position operator x acting on a density matrix ρ has the correspondence

$$\begin{aligned} g(x)\rho \leftrightarrow & g\left(x+\frac{i\hbar}{2}\frac{\partial}{\partial p}\right)W(x,p) = \sum_{n=0}^{\infty}\frac{g^{(n)}(0)}{n!}\left(x+\frac{i\hbar}{2}\frac{\partial}{\partial p}\right)^n W(x,p) \\ =& \sum_{n=0}^{\infty}\frac{g^{(n)}(0)}{n!}\sum_{l=0}^{n}\frac{n!}{l!(n-l)!}x^{n-l}\left(\frac{i\hbar}{2}\frac{\partial}{\partial p}\right)^l W(x,p) \\ =& \sum_{l=0}^{\infty}\frac{1}{l!}\sum_{n=l}^{\infty}\frac{g^{(n)}(0)}{(n-l)!}x^{n-l}\left(\frac{i\hbar}{2}\frac{\partial}{\partial p}\right)^l W(x,p) \\ =& \sum_{l=0}^{\infty}\frac{1}{l!}\frac{\partial^l g(x)}{\partial x^l}\left(\frac{i\hbar}{2}\right)^l\frac{\partial^l}{\partial p^l}W(x,p), \end{aligned} \tag{A.1}$$

where we used the notation $g^{(n)}(0) = \left.\frac{\partial^n g(x)}{\partial x^n}\right|_{x=0}$. Similarly, we obtain

$$\rho g(x) \leftrightarrow g\left(x-\frac{i\hbar}{2}\frac{\partial}{\partial p}\right)W(x,p) = \sum_{l=0}^{\infty}\frac{1}{l!}\frac{\partial^l g(x)}{\partial x^l}\left(-\frac{i\hbar}{2}\right)^l\frac{\partial^l}{\partial p^l}W(x,p). \tag{A.2}$$

The correspondences for commutator and anti-commutator are

$$[g(x),\rho] \leftrightarrow \sum_{l\in 2\mathbb{N}+1}\frac{2}{l!}\frac{\partial^l g(x)}{\partial x^l}\left(\frac{i\hbar}{2}\right)^l\frac{\partial^l}{\partial p^l}W(x,p) \tag{A.3a}$$

$$\{g(x),\rho\} \leftrightarrow \sum_{l\in 2\mathbb{N}}\frac{2}{l!}\frac{\partial^l g(x)}{\partial x^l}\left(\frac{i\hbar}{2}\right)^l\frac{\partial^l}{\partial p^l}W(x,p). \tag{A.3b}$$

Appendix B.

Stable particle configurations in the single-frequency case for N atoms

We apply the stability criterion discussed in section 3.7 on the simple case of N atoms within a single-mode field while neglecting U_0 and for $\delta_c < 0$. The equilibrium points have to fulfil the single-mode form of equation (4.2)

$$F_i \propto \sum_l \cos(kx_i)\sin(kx_l) = 0 \qquad \forall i. \tag{B.1}$$

Hence we need that either

1. $\cos(kx_i) = 0\ \forall i$ or
2. $\cos(kx_i) \neq 0$ for at least one i and $\sum_l \sin(kx_l) = 0$.

From $F_i \propto \sum_l \sin(kx_l)\cos(kx_i)$ we get the Jacobian

$$\mathcal{J}_{ij} = \frac{\partial F_i}{\partial x_j} \propto \cos(kx_i)\cos(kx_j) - \delta_{ij}\sin(kx_i)\sum_l \sin(kx_l). \tag{B.2}$$

For the stability criterion we need to calculate the eigenvalues of this matrix.

Case 1

As $\cos(kx_i) = 0$ we have $\sin(kx_i) = \pm 1$. The Jacobian is diagonal, so the eigenvalues are the diagonal elements

$$\lambda_i = -\sin(kx_i)\sum_l \sin(kx_l). \tag{B.3}$$

There are three different scenarios:

- If all $\sin(kx_i)$ are the same (e.g. all +1 or all -1) we get $\lambda_i < 0\ \forall i$. Hence those points are stable.

- In the balanced scenario (same number of +1 and -1) we get $\lambda_i = 0$ and we can't make a conclusion about the stability. However, as $\sum_l \sin(kx_l) = 0$ those points are included in case 2 and the classification can be postponed.
- Otherwise (unbalanced) we always get $\lambda_i > 0$ for at least one i. These points are unstable.

Case 2

As the matrix with the entries $\mathcal{J}_{ij} = \cos(kx_i)\cos(kx_j)$ is the product of one vector with itself, all but one eigenvalues are zero. The non-zero eigenvalue is the normalisation squared of this vector, hence

$$\lambda_1 = \sum_l \cos^2(kx_l).$$

As at least one $\cos(kx_i) \neq 0$ we have $\lambda_1 > 0$ and all equilibrium points obtained by case 2 are unstable.

Thus the only stable points are fulfilling $\cos(kx_i) = 0$ and $\sin(kx_i) = 1$ or $\sin(kx_i) = -1$ for all i. That is $kx_i = \pi/2 + 2m\pi$ or $kx_i = 3\pi/2 + 2m\pi$ for all i ($m \in \mathbb{Z}$) which are in the diagonal of the N-dimensional space.

Appendix C.

Dimensionless form of the equations of motion

For numerical simulations we need to work with the dimensionless equations of motion. For this we want to consider dimensionless quantities. Spatial quantities are transformed with k and time quantities with $\omega_R = \frac{\hbar k^2}{2m}$. A system is then fully determined by choosing the dimensionless quantities, k and ω_R (or m). Specifically, we get

- position: $x_j \to k x_j$
- momentum: $p_j \to \frac{p_j}{\hbar k}$
- spatial frequency: $k_n = nk \to n$
- time: $t \to \omega_R t$
- frequencies: e.g. $U_0 \to \frac{U_0}{\omega_R}$
- field: $\alpha_n \to \alpha_n$

This leads to the coupled equations of motion (3.26)

$$\frac{\mathrm{d}(kx_j)}{\mathrm{d}(\omega_R t)} = 2\frac{p_j}{\hbar k} \tag{C.1a}$$

$$\frac{\mathrm{d}\left(\frac{p_j}{\hbar k}\right)}{\mathrm{d}(\omega_R t)} = -\sum_n n\left(\frac{U_0}{\omega_R}|\alpha_n|^2 \sin(2nkx_j) + \frac{\eta_n}{\omega_R}(\alpha_n + \alpha_n^*)\cos(nkx_j)\right) \tag{C.1b}$$

$$\frac{\mathrm{d}\alpha_n}{\mathrm{d}(\omega_R t)} = i\left(\frac{\delta_c}{\omega_R} - \frac{U_0}{\omega_R}\sum_j \sin^2(nkx_j)\right)\alpha_n - \frac{\kappa}{\omega_R}\alpha_n - i\frac{\eta_n}{\omega_R}\sum_j \sin(nkx_j). \tag{C.1c}$$

For the over-damped motion (3.30) we obtain

$$\frac{\mathrm{d}(kx_j)}{\mathrm{d}(\omega_R t)} = -2\frac{\omega_R}{\mu}\sum_n n\left(\frac{U_0}{\omega_R}|\alpha_n|^2 \sin(2nkx_j) + \frac{\eta_n}{\omega_R}(\alpha_n + \alpha_n^*)\cos(nkx_j)\right), \tag{C.2}$$

with the field in the steady state (3.28)

$$\alpha_n = \frac{\eta_n}{\omega_R} \frac{\sum_j \sin(nkx_j)}{\frac{\delta_c}{\omega_R} - \frac{U_0}{\omega_R}\sum_j \sin^2(nkx_j) + i\frac{\kappa}{\omega_R}}. \tag{C.3}$$

Bibliography

[1] Immanuel Bloch. Ultracold quantum gases in optical lattices. *Nature Physics*, 1(1):23–30, 2005.

[2] Peter Domokos and Helmut Ritsch. Mechanical effects of light in optical resonators. *Journal of the Optical Society of America B Optical Physics*, 20:1098–1130, 2003.

[3] Peter Horak, Gerald Hechenblaikner, Klaus M Gheri, Herwig Stecher, and Helmut Ritsch. Cavity-induced atom cooling in the strong coupling regime. *Physical review letters*, 79(25):4974, 1997.

[4] Vladan Vuletić and Steven Chu. Laser cooling of atoms, ions, or molecules by coherent scattering. *Physical Review Letters*, 84(17):3787, 2000.

[5] Peter Domokos and Helmut Ritsch. Collective cooling and self-organization of atoms in a cavity. *Physical Review Letters*, 89(25):253003, 2002.

[6] Adam T Black, Hilton W Chan, and Vladan Vuletić. Observation of collective friction forces due to spatial self-organization of atoms: from rayleigh to bragg scattering. *Physical Review Letters*, 91(20):203001, 2003.

[7] JK Asbóth, P Domokos, H Ritsch, and A Vukics. Self-organization of atoms in a cavity field: Threshold, bistability, and scaling laws. *Physical Review A*, 72(5):053417, 2005.

[8] Wolfgang Niedenzu, Tobias Grießer, and Helmut Ritsch. Kinetic theory of cavity cooling and self-organisation of a cold gas. *EPL (Europhysics Letters)*, 96(4):43001, 2011.

[9] Benjamin L Lev, András Vukics, Eric R Hudson, Brian C Sawyer, Peter Domokos, Helmut Ritsch, and Jun Ye. Prospects for the cavity-assisted laser cooling of molecules. *Physical Review A*, 77(2):023402, 2008.

[10] Sebastian Krämer and Helmut Ritsch. Self-ordering dynamics of ultracold atoms in multicolored cavity fields. *Phys. Rev. A*, 90:033833, 2014.

[11] Peter Domokos, Thomas Salzburger, and Helmut Ritsch. Dissipative motion of an atom with transverse coherent driving in a cavity with many degenerate modes. *Physical Review A*, 66(4):043406, 2002.

[12] Sarang Gopalakrishnan, Benjamin L Lev, and Paul M Goldbart. Emergent crystallinity and frustration with bose–einstein condensates in multimode cavities. *Nature Physics*, 5(11):845–850, 2009.

[13] Michael M Burns, Jean-Marc Fournier, and Jene A Golovchenko. Optical matter: crystallization and binding in intense optical fields. *Science*, 249(4970):749–754, 1990.

[14] Kishan Dholakia and Pavel Zemánek. Colloquium: gripped by light: optical binding. *Reviews of Modern Physics*, 82(2):1767, 2010.

[15] Stefan Ostermann, Matthias Sonnleitner, and Helmut Ritsch. Scattering approach to two-colour light forces and self-ordering of polarizable particles. *New Journal of Physics*, 16(4):043017, 2014.

[16] Valentin Torggler and Helmut Ritsch. Adaptive multifrequency light collection by self-ordered mobile scatterers in optical resonators. *Optica*, 1(5):336–342, 2014.

[17] Claude N Cohen-Tannoudji. Nobel lecture: Manipulating atoms with photons. *Rev. Mod. Phys.*, 70:707–719, Jul 1998.

[18] Theodor W Hänsch and Arthur L Schawlow. Cooling of gases by laser radiation. *Optics Communications*, 13(1):68–69, 1975.

[19] EL Raab, M Prentiss, Alex Cable, Steven Chu, and D E Pritchard. Trapping of neutral sodium atoms with radiation pressure. *Physical Review Letters*, 59(23):2631, 1987.

[20] Dieter Jaksch, Ch Bruder, Juan Ignacio Cirac, Crispin W Gardiner, and Peter Zoller. Cold bosonic atoms in optical lattices. *Physical Review Letters*, 81(15):3108, 1998.

[21] Edwin T Jaynes and Frederick W Cummings. Comparison of quantum and semiclassical radiation theories with application to the beam maser. *Proceedings of the IEEE*, 51(1):89–109, 1963.

[22] Wolfgang Niedenzu. *Microscopic description and simulation of ultracold atoms in optical resonators*. PhD thesis, Universität Innsbruck, 2012.

[23] Peter Domokos, Peter Horak, and Helmut Ritsch. Semiclassical theory of cavity-assisted atom cooling. *Journal of Physics B: Atomic, Molecular and Optical Physics*, 34(2):187, 2001.

[24] Gerald Hechenblaikner, Markus Gangl, Peter Horak, and Helmut Ritsch. Cooling an atom in a weakly driven high-q cavity. *Physical Review A*, 58(4):3030, 1998.

[25] Daniel F Walls and Gerard J Milburn. *Quantum Optics*. SpringerLink: Springer e-Books. Springer, 2008.

[26] Ravinder R Puri. *Mathematical Methods of Quantum Optics*. Physics and astronomy online library. Springer, 2001.

[27] Helmut Ritsch, Peter Domokos, Ferdinand Brennecke, and Tilman Esslinger. Cold atoms in cavity-generated dynamical optical potentials. *Reviews of Modern Physics*, 85(2):553, 2013.

[28] Wolfgang P Schleich. *Quantum Optics in Phase Space*. Wiley, 2011.

[29] Crispin W Gardiner and Peter Zoller. *Quantum Noise: A Handbook of Markovian and Non-Markovian Quantum Stochastic Methods with Applications to Quantum Optics*. Springer Series in Synergetics. Springer, 2004.

[30] Crispin W Gardiner. *Stochastic Methods: A Handbook for the Natural and Social Sciences*. Springer Series in Synergetics. Springer Berlin Heidelberg, 2010.

[31] W.E. Boyce and R.C. DiPrima. *Elementary Differential Equations and Boundary Value Problems*. John Wiley & Sons, Incorporated, 2013.

[32] CJ Hood, TW Lynn, AC Doherty, AS Parkins, and HJ Kimble. The atom-cavity microscope: Single atoms bound in orbit by single photons. *Science*, 287(5457):1447–1453, 2000.

[33] P Horak, H Ritsch, T Fischer, P Maunz, T Puppe, PWH Pinkse, and G Rempe. Optical kaleidoscope using a single atom. *Physical review letters*, 88(4):043601, 2002.

[34] Sarang Gopalakrishnan, Benjamin L Lev, and Paul M Goldbart. Exploring models of associative memory via cavity quantum electrodynamics. *Philosophical Magazine*, 92(1-3):353–361, 2012.